Basalt geochemistry and mantle flow during early backarc basin evolution: Havre Trough and Kermadec Arc, southwest Pacific

J. Gill[1*], K. Hoernle[2,3], E. Todd[4], F. Hauff[2], R. Werner[2], C. Timm[2], D. Garbe-Schönberg[3], M. Gutjahr[2]

[1] University of California, Santa Cruz, CA 95064, USA

[2] GEOMAR Helmholtz Centre for Ocean Research, Kiel 24148, Germany

[3] Institute of Geosciences, Kiel University, 24118 Kiel, Germany

[4] U.S. Geological Survey, Alaska Science Center, Anchorage, AK 99508, USA

*Corresponding author: James Gill (gillord@ucsc.edu) ORCID 0000-0003-2584-9687

Hoernle ORCID 0000-0002-3165-3480

Hauff ORCID 0000-0001-9503-9714

Todd ORCID 0000-0002-4871-9730

Garbe-Schönberg ORCID 0000-0001-9006-9463

Key Points:

- The Havre Trough is now one of the most thoroughly analyzed backarc basins
- Mantle beneath a backarc basin is replaced quickly even during the rifting stage before spreading starts
- Slab components during the rifting stage are similar to those during spreading but are more disorganized during rifting

Index Terms:

- 8170 Subduction zone processes
- 8178 Tectonics and magmatism
- 1038 Mantle processes
- 1040 Radiogenic isotope geochemistry

• 8440 Calderas

Abstract

The Havre Trough backarc basin in the southwest Pacific is in the rifting stage of development. We distinguish five types of basalt there based on their amount and kind of slab component: backarc basalts (BAB) with little or no slab component; modified BAB (mBAB) with slight amounts; reararc (RA) with more; remnants of the pre-existing arc (Colville Ridge horsts, CRH); and arc front volcanoes within the Havre Trough. Previous sub-arc mantle is quickly removed and replaced by more fertile mantle with less slab component. The ambient mantle is "Pacific" isotopically, and more enriched in Nb/Yb and Nd and Hf isotope ratios north of the Central Kermadec Discontinuity at 32°S than to the south. The contrast may reflect inheritance in the south of mantle that was depleted during spreading that formed the southern South Fiji Basin, and a higher degree of melting because of a wetter slab-derived flux. The slab component also differs along strike, more like a dry melt in the north and a super-critical fluid in the south. The mass fraction of slab component increases southward in the backarc as well as the arc front. Reararc volcanoes have the most slab component (1-2%) and form indistinct ridges at high angles to, and <50 km behind, frontal volcanoes. Backarc basalts have less and occur throughout the basin. Slab components are distributed further into the backarc, and more irregularly, during the rifting than spreading stage of backarc basin development. The rifting stage is disorganized geochemically as well as spatially. [248 words]

Plain Language Summary

Island arcs split as do continents, with new ocean crust forming between the rifted parts. Splitting progresses from early rifting to mature spreading stages. We present the most thorough geochemical data yet for volcanic rocks erupted during the rifting stage of one of these events. We found that they are derived from new mantle that flowed quickly into the system to replace what fed the arc. The new mantle is more inherently fertile but has

fewer additions from the subducting slab than what fed the arc. Both the mantle and slab components differ north versus south of a major tectonic boundary within the basin at 32°S. The slab components are similar during both the rifting stage in the Havre Trough and spreading stage elsewhere, but are distributed or tapped differently, being more irregular during rifting. Rifting leaves permanent geochemical records that modulate the geochemical evolution of arc crust that can be added to continents. [154 words]

1 Introduction

This paper presents new data for volcanic rocks dredged from the Kermadec Quaternary volcanic front (QVF) and Havre Trough (HT) north of New Zealand from 28° to 35°S (~700 km), a distance longer than the Central and Eastern Spreading Centers in the Lau Basin combined or 75% the length of the Mariana Trough.

At the beginning of the plate tectonics concept, the Lau Basin and Havre Trough were the first backarc basins to be recognized as forming between halves of intra-oceanic island arcs in a fashion similar to the major ocean basins (Karig, 1970). The Tonga-Kermadec Ridges are the residual frontal arcs; the Lau-Colville Ridges are the remnant arcs. Rifting of arcs and continents results in mantle upwelling, and eventually leads to seafloor spreading that separates parts of the arc or continent. Chief differences between the two include the thicker crust and lithosphere, more felsic crust, and drier mantle in the continental case. Other differences are that backarc basin formation can repeat itself at tens of million year intervals (e.g., first the Parece Vela Basin, then the Mariana Trough in the northern hemisphere; or the South Fiji Basin, then the Lau and North Fiji Basins in the southern), and that frontal arc volcanism apparently wanes but remnant arc volcanism continues during backarc basin rifting (Martinez and Taylor, 2006; Gill, 1976).

Numerical models of backarc basin formation predict spatial and temporal patterns of mantle flow and magmatism (e.g., Honda et al., 2007; Lin et al., 2010; Magni, 2019) that are difficult to test without geophysical, geochemical, and geochronological data for submarine areas and rocks. This is especially true for the earliest phase of backarc basin formation that usually is referred to as the "rifting stage", and is thought to characterize the western Lau and North Fiji Basins, and the northernmost Mariana Trough (e.g., Parson and Hawkins, 1994; Martin, 2013; Martinez et al., 1995). The active

rift and backarc knolls regions of the Izu arc (e.g., Hochstaeder et al., 2001; Ishizuka et al., 2003) and the Havre Trough (e.g., Malahoff et al., 1982; Wright et al., 1996; Wysoczanski et al., 2010) are now the best studied examples of this stage.

Although the Havre Trough usually is thought to represent rifting or "disorganized spreading" (Wysoczanski et al., 2010), others have argued that it started with seafloor spreading characterized by oceanic crust with conventional magnetic anomalies (Malahoff et al., 1982; Tontini et al., 2019), or that it is mostly floored by foundered arc crust (Katz, 1978). A reararc chain of seamounts with arc-like geochemistry at ~36°S suggests the presence of "hot fingers" in the Havre Trough (Todd et al., 2011; Kim and Lee, 2018) as in northeast Japan during the Quaternary and in the Izu arc during the Neogene (Tamura et al., 2002; Honda et al., 2007).

For these reasons, the six-week GEOMAR SO255 expedition was undertaken in the Kermadec Arc – Havre Trough (KAHT) system in April-May 2017, from the trench to the remnant arc. This paper reports its results for the Quaternary Volcanic Front and Havre Trough. A companion paper presents results for the older Kermadec and Colville Ridges (Hoernle et al., In Rev). Rock analyses for both studies are compiled in Hauff et al. (2020). Throughout this paper, the acronym QVF refers solely to the Kermadec Quaternary Volcanic Front.

2 Background

The Kermadec arc is the southern half of the Tonga-Kermadec arc system that extends ~2600 km from near Samoa in the north to New Zealand in the south (Fig. 1). The boundary between the Tonga and Kermadec arcs is where the Louisville Ridge currently intersects the trench at 25°S. From east to west, the Kermadec system consists of the frontal forearc and arc (Kermadec Ridge ± QVF), backarc basin (Havre Trough), and remnant arc (Colville Ridge). The Tongan equivalents are the Tonga Ridge, Lau Basin, and Lau Ridge (Fiji). Prior to formation of the Lau Basin and Havre Trough, the combined arc system constituted the Vitiaz Arc (Gill and Gorton, 1973; Coleman and Packham, 1976).

In the Kermadec sector, ~80-125 Ma old Pacific Plate lithosphere formed at the Osborne Trough (Mortimer et al., 2019) subducts beneath the Australian Plate at 6.5 to 5

cm/year, decreasing southward, with a convergence angle almost east-west (DeMets et al., 1994), although the relative and absolute velocities and vector depend on the plate circuit used (e.g., van de Lagemaat et al., 2018). At 30°S, Syracuse et al. (2010) give a relative velocity of 6.5 cm/yr, a dip angle of 56°, and depth to the slab beneath the volcanic front of 170 km that is unusually deep. Their resulting thermal parameter ϕ and slab surface temperature beneath the arc are 57 and 773°C, respectively, which would be high enough to melt both the 200-m-thick subducting sediments and basaltic crust if they are water-saturated, even in this colder-than-average arc. The convergence rate and dip angle, and therefore the thermal parameter, all decrease southward toward New Zealand, resulting in higher slab surface temperatures and shallower dehydration (van Keken et al., 2011). The subducting plate lies 170-450 km beneath the Havre Trough. It shoals and steepens between 28° and 32°S, with a large cluster of intermediate depth earthquakes (200-450 km) beneath the Havre Trough at ~30°S (e.g., Hayes et al., 2018). Because a low velocity slab persists to ~1000 km in tomographic images (van de Lagemaat et al., 2018), the apparent shoaling may reflect warming as the slab surface temperature increases southward.

Fig.1

In the northern part of our study area, from 28°S to 32°S, the Havre Trough is 130-150 km wide. In the east, hundreds of knolls are present even on satellite bathymetry, defining irregular NW-trending ridges behind QVF volcanoes and between small sedimented basins (Fig. 2). The ridges are similar in length to, but less distinct than, the rear arc seamount chains behind the Izu arc (e.g., Hochstaedter et al., 2001). We sampled both the ridges and basins, from 800-2300 mbsl. In contrast, the western half of the Havre Trough is 2500 m deep on average at this latitude, and has more subdued relief with several buried, apparently faulted ridges that have relief of 1.0-1.5 km beneath 180-800 m of sediment (Bassett et al., 2016, Fig.4; Tontini et al., 2019, Fig 3). Therefore, there seems to have been more young volcanism in the eastern half of the basin.

The crust beneath the Havre Trough at these latitudes is ~10-13 km thick, and thinner than beneath the arc (16 ±1 km) (Bassett et al., 2016). It has a thin middle crust with Vp=6.0-6.4 km/sec, thick lower crust with Vp=6.8-7.0 km/sec, and uppermost mantle with Vp=8.1 km/sec. Thus, the velocity structure of the Havre Trough crust is still

quite arc-like despite being thinner, but the mantle already has typical mid-oceanic velocity.

The southern part of our study area, from 32°S to 35°S, starts at the Central Kermadec Discontinuity (CKD) where the water depth of the entire arc system deepens abruptly from forearc to remnant arc, and the Tongan and Lau arc substrates may end beneath the Kermadec and Colville Ridges (Bassett et al., 2016). The Havre Trough reaches an average depth of ~3700 m, a global maximum for an active backarc basin. The Havre Trough crust is 1-4 km thinner than further north but has a similar velocity structure (Bassett et al., 2016, Figs. 5, 6). The western half is again characterized by less relief and more sediment. Tontini et al. (2019) suggested that this western half is underlain by crust formed by seafloor spreading at 5.9 to 2.6 Ma based on their interpretation of magnetic anomalies. However, dated volcanic rocks on the sea floor are as young in the west as the east (Wysoczanski et al., 2019); most magnetic anomalies are discontinuous, cannot be identified uniquely on multiple crossings (Fujiwara et al., 2001), and have not been modeled for specific reversal sequences; and apparent horsts of the former arc are present within or near the location of the magnetic anomalies (Section 4.4). Therefore, we suggest caution with this interpretation.

The more detailed bathymetry available for this southern region reveals a northeasterly fabric that cuts across indistinct ridges and basins (Fujiwara et al., 2001, Fig. 2; Tontini et al., 2019, Fig. 2a). Coalesced volcanoes in the eastern half of the Havre Trough at 34.5°S maintain this fabric. We refer to this feature as the Kibblewhite Ridge, because it extends from Kibblewhite Seamount at the volcanic front to Rapuhia Seamount and Ridge in the western basin, and is similar to the Rumble V Ridge at 36°S.

Havre Trough basalts are difficult to date because they have low K, and are vesicular and glassy. Nevertheless, Ar-Ar ages for crystalline groundmass have been published for thirteen basalts from almost the full width of the Havre Trough, and from 30° to 36°S (Mortimer et al., 2007; Wysoczanski et al., 2019). Five ages are <100 ka, and the rest are 0.4-1.2 Ma. Therefore, surface volcanic edifices throughout the Havre Trough are ≤1.5 Ma. The only potential horsts of older basement are close to the remnant arc (Section 4.4), and ages do not decrease west to east as predicted by Wright et al. (1996)

and Tontini et al. (2019). Drilling would be necessary to determine the maximum age of the basement.

The QVF lies on the Kermadec Ridge north of L'Esperance Rock at 31.3°S, but it steps 20 km westward into the Havre Trough at the Central Kermadec Discontinuity (de Ronde et al., 2007). We sampled near four of the volcanoes south of the Central Kermadec Discontinuity – Kibblewhite, Cole, Kuiwai, and Haungaroa, from south to north – for which there are no previously published major and trace element and isotope analyses of the same sample.

The preceding summary illustrates the complexity inherent in discussions of what lies *within* versus *behind* a volcanic arc. For some purposes, the only distinction that matters is between the arc and a backarc basin behind it that is characterized by active seafloor spreading (e.g., Tonga or Marianas) and by "back arc basin basalts" (BABB: Sinton and Fryer, 1987). However, most volcanic arcs include what are called "reararc" (RA) volcanoes in which magmas resemble arcs in composition yet differ from those in the edifices defining the volcanic front (those closest to the convergent plate boundary). This results in the across-arc geochemical trends that have been recognized for at least 70 years, such as increasing K_2O contents relative to SiO_2 (e.g., Gill, 1981, chapter 6).

Later we will discuss the geochemical differences between QVF and RA lavas. Accordingly, in Fig. 2 we identify two active volcanoes, Giggenbach and Havre, as RA. They usually are included in the Kermadec arc but they are located behind Macauley volcano and L'Esperance Rock, respectively, and are farther from the plate boundary than the other active volcanoes. We also apply the RA name to some of our dredged samples. In the north, the QVF lies on the Kermadec Ridge whereas the RA volcanoes are in the Havre Trough, up to 30 km behind the QVF. In the south, both the QVF and RA volcanoes lie in the Havre Trough, so the distinction is geochemical, and RA-type magmas extend the full width of the Havre Trough.

There are no unequivocal morphological or geochemical criteria by which to distinguish "reararc" from "backarc" volcanoes. However, the "reararc" ones often are larger and shallower. Todd et al. (2011) distinguished between "rift-type" versus "arc-type" magmas within the southern Havre Trough, and attributed the difference to variable slab surface temperature that resulted in a lower temperature fluid-like slab component in

"rift-type" magmas versus a higher temperature melt-like slab component in "arc-type" magmas. In the Izu reararc, Hochstaedter et al. (2001) and others distinguished chains of older seamounts characterized by "arc-type" lavas, versus younger, isolated, smaller knolls with "rift-type" lavas. Subsequently, Heywood et al. (2020), based on updated information, abandoned correlations between geochemistry, morphology, and age behind the Izu volcanic front, and replaced them with a simple distinction based solely on La/Yb ratios that are higher in "arc-type" samples. With this in mind, we will discuss in a later section how basalt geochemistry, location, and bathymetry vary together within the Havre Trough.

On the subducting Pacific Plate, the 12-15 km-thick Hikurangi Plateau (Fig. 1), a Cretaceous Large Igneous Province, is thought to be actively subducting south of the Rapuhia Scarp at 35°S (Collot and Davy, 1998; Reyners et al., 2011). It may be underlain by up to 25 km of serpentinized mantle (Herath et al., 2020), and is overlain by seamounts with HIMU-like isotopes (Hoernle et al., 2010) that may contribute to QVF magmas as far north as 32°S (Timm et al., 2014).

One last important background concept is the Ambient Mantle Wedge (AMW), a term discussed by Woodhead et al. (2012) and applied to the KAHT by Todd et al. (2010, 2011). It refers to what the mantle wedge composition was like before adding a subduction component. We will add our Havre Trough data to Todd et al.'s (2011), and show that the AMW of the Havre Trough and South Fiji and Norfolk Basins is similar to the source of East Pacific Rise MORB. Todd et al. (2012) found that such ambient mantle underlay the entire Vitiaz Arc prior to its dismemberment by opening of the North Fiji and Lau Basins.

3 Samples and analytical methods

We studied 165 volcanic rock samples dredged from 56 sites in the Havre Trough and Kermadec volcanic front during the GEOMAR SO255 expedition in 2017. Sample descriptions, and bathymetric maps of the dredge sites and dredge tracks, are presented in Hoernle et al. (2017). Dredge locations are also shown in Fig. 2. Unless otherwise identified, all DR-numbers in this paper refer to SO255 samples. All were analyzed for major elements by XRF, most for trace elements by solution ICPMS, about half for Sr,

Nd, and Pb isotopes, and 27 for Hf, making the Havre Trough now one of the most thoroughly analyzed of any backarc basin. Data for other SO255 samples, from the older Kermadec and Colville Ridges, are discussed by Hoernle et al. (In Rev.) and included in Hauff et al. (2020).

Fig. 2

Whole rock samples are fresh interiors of lava or clasts that were cleaned in deionized water, dried at 50°C, crushed to cm-size chips in a steel jaw crusher, hand-picked under a binocular microscope, soaked repeatedly in distilled water, and pulverized in agate prior to analysis. Glass from some samples was analyzed by LA-ICPMS. Rock from the 0.5-1 mm fraction, or glass chips, were used for isotope analysis after leaching in 2N HCl for 1 hour at 70°C prior to dissolution.

Our analytical methods, precision, and accuracy are described in detail in Hauff et al. (2020), and are the same as for other data from SO255 (Timm et al., 2019; Hoernle et al., In Rev.). All major element data in the tables, figures, and text are presented on an anhydrous basis with $FeO(T)$ recalculated from $Fe_2O_3(T)$; the original LOI and sum are included in Table 1 for reference.

4 Results

Analyses are given in Table 1. We distinguish four geochemically different types of basalt within the Havre Trough in addition to rocks from the QVF. They are: Back Arc Basalt (BAB); slightly modified Back Arc Basalt (mBAB); Rear Arc (RA); and Colville Ridge Horst (CRH). We further distinguish between two sub-types of mBAB and RA depending on whether they are from north or south of the Central Kermadec Discontinuity: i.e., mBAB-N and –S; and RA-N and –S. We discuss them separately below.

4.1 Backarc Basalt (BAB)

BAB have so little slab component that we use them to refine the composition of AMW of Todd et al. (2011). The BAB group rocks are similar to Eastern Pacific Rise (EPR) N- to E-MORB with 6-9 wt% MgO, K_2O/TiO_2=0.15-30, and Ti-enrichment with decreasing MgO (Fig. 3). They overlap, or plot slightly above EPR MORB arrays, in

La/Yb, Th/Yb, and Ba/Yb versus Nb/Yb diagrams (Fig. 4), and have Sm/Hf ratios ~1.5 (i.e., no Hf concentration anomaly: Fig. 5b). An important difference is that BAB HREE patterns are slightly steeper than N- and E-MORB relative to their LREE enrichment (Dy_N/Yb_N >1.15 at La_N/Sm_N <1.5: Fig. 5a), and the overall pattern is S-shaped with a maximum at Nd and slight minimum at Tm (Fig. 5d). Even their Pb-Sr-Nd-Hf isotopes are surprisingly like those of EPR N- to E-MORB, with Pb near the Northern Hemisphere Reference Line (NHRL) and Hf below the Terrestrial Array (Figs. 6-8). However, their negative correlation between $^{143}Nd/^{144}Nd$ and Nb/Yb ratios is offset to lower Nb/Yb, or vice versa, than for EPR MORB (Fig. 6a).

Fig. 3+4

When defined so conservatively, only 12 basalts from our DR68, 69, 109, and 160-4 qualify as BAB. Literature data for SO135-18DR and 19DR-2 from near our DR109 (Haase et al., 2002) also qualify as BAB. PPTUW/5, the best-known and previously the most depleted basalt from the Havre Trough, is another example but its location has been uncertain (Gamble et al., 1996; Woodhead et al., 2001). Apparently, it was from Dredge 39 in the Ngatoroirangi Rift during Leg 5 of SIO Expedition PPTUW led by Harmon Craig in 1986. Tholeiitic basalts from DSDP Site 285 and the Alison and Julia Seamounts in the South Fiji Basin, plus alkali basalts from the Coquille and Marion Seamounts in the South Fiji Basin and one from the Norfolk Basin (Mortimer et al., 2007; Todd et al., 2011), define the rest of the regional AMW.

Fig. 5+6

Our new samples include the most depleted example of the AMW thus far discovered (DR160-4; Nb/Yb=0.14). However, most of our BAB are more enriched than previously known with Nb/Yb = 1.5-2.5, and that range sometimes occurs even in one location (DR68). The two BAB from south of the Central Kermadec Discontinuity are more depleted than those to the north of it in Nb/Yb and Nd and Hf isotope ratios.

4.2 Modified Backarc Basalt (mBAB)

Most Havre Trough mBAB samples have slightly more arc-like features in one or more of the geochemical criteria listed above. That is, one or more of (Ba,Th,La)/Yb relative to Nb/Yb ratios lie farther above the MORB array in Fig. 4, their Nd isotopes lie

below the AMW relative to Nb/Yb and Hf isotope ratios (Fig. 6), and Pb isotopes in mBAB-N lie above the NHRL but below the QVF field (Fig. 7). We refer to these basalts as modified BAB (mBAB), and we separate those from north of the Central Kermadec Discontinuity (mBAB-N) from those to the south (mBAB-S). Samples qualifying as mBAB from other sites in the Havre Trough have been studied previously. In the north they are SO135-19DR-1 and 41DR-3, and P63474 that was dated at 1.1 Ma (Haase et al., 2002; Mortimer et al., 2007). In the south they are SIO D41D-A and basalts from the Ngatoroirangi, Rumble, and Ngatoro Rifts (Wysoczanksi et al., 2006; Todd et al., 2010, 2011). All Ar-Ar dates of mBAB are <0.7 Ma (Wysoczanski et al., 2019). Most of our mBAB appear young and fresh.

Fig. 7

Combining our new samples with literature data, mBAB are present for at least 650 km along the Havre Trough which is more extensive than the Central and East Lau Spreading Centers combined. The mBAB group shares many geochemical features with rocks from the southern East Lau Spreading Center as it approaches the Tongan arc, whereas BAB are more like basalts from the Central Lau Spreading Center. Most mBAB are from near the middle of the Havre Trough, 50-70 km behind the QVF, near the western edge of the seamount terrane. However, one BAB and one mBAB are from deep basins less than 50 km behind the volcanic front (DR109 and 174, respectively). Most mBAB are from basins as opposed to ridges, the most prominent being a NW-trending basin behind Haungaroa, just south of the Central Kermadec Discontinuity. That is, basalts with little slab component are widespread even during the rifting stage of the Havre Trough, and occur within the width of a typical volcanic arc (~70 km).

Fig. 8

4.2.1 Modified Backarc Basalt North of the Central Kermadec Discontinuity (mBAB-N)

We analyzed 26 mBAB-N samples from 10 sites. Like BAB, their major elements are most similar to EPR N-MORB and basalts of the Central Lau Spreading Center. Some are as Fe-enriched as MORB, and TiO_2 is only slightly lower relative to MgO. Na_2O and TiO_2 are higher than in either QVF or RA, or even mBAB-S.

mBAB-N are from relatively enriched AMW. With one exception, their Nb/Yb ratios range from 0.5 to 3.3 mostly like D- to N-MORB, and are higher than for QVF and RA. Because all are tholeiitic basalts, and their negative correlation between Nb/Yb and $^{143}Nd/^{144}Nd$ is close to that of AMW, this wide range in Nb/Yb reflects variable mantle enrichment rather than just variable percent melting. In one case (DR147) there is a 50% range in Nb/Yb at one dredge site. Relative to Nb/Yb, their Ba/Yb and Th/Yb ratios are slightly higher than AMW and MORB values (Fig. 4), and their $^{143}Nd/^{144}Nd$ ratios are slightly lower. Ce/Pb ratios are 7-17, higher than in the QVF but lower than in MORB (Fig. 8). Pb isotopes also show slight effects of an added slab component, with ratios intermediate between the BAB and QVF fields (Fig. 7). We use this intermediacy as a defining feature of mBAB-N because some trace element enrichments are ambiguous. Most Sr and Nd isotope ratios overlap those of EPR N- and E-MORB, with $^{143}Nd/^{144}Nd$ ~0.51303-0.51308 (Fig. 6b).

Like BAB, most mBAB-N have S-shaped REE patterns with steeper HREE patterns than QVF or MORB (i.e., higher Dy/Yb ratios: Fig. 5), and they also have the highest Zr/Hf ratios in the Havre Trough (38-50) that are similar to E-MORB (Fig. 5). mBAB-N with the greatest La and Th enrichments also have small (~15%) negative Hf concentration anomalies, a negative correlation that applies to most Havre Trough basalts, reaching 50% negative anomalies in the most LREE-enriched RA-N at Gill volcano.

4.2.2 Modified Backarc Basalt South of the Central Kermadec Discontinuity (mBAB-S)

We analyzed 20 mBAB-S samples from 9 sites, mostly mid-way across the Havre Trough from 32 to 34.5°S. However, they are found as close as 20 km to the volcanic front at DR174 behind Ngatoroirangi Seamount, to as far as 110 km from it at DR160 behind Haungaroa Seamount. That is, their distance from the QVF overlaps with RA-S lavas. Most are low-K tholeiitic basalts, but almost half are basaltic andesites, and they have lower TiO_2 and FeO* relative to MgO than mBAB-N (Fig. 3). They are more depleted than mBAB-N, with LREE-depletion, Nb/Yb ratios = 0.2-1.0, Zr/Hf = 30-40, $^{143}Nd/^{144}Nd > 0.51308$, and $^{176}Hf/^{177}Hf > 0.28315$. They also have flatter HREE than

mBAB-N (Fig. 5). They show evidence of small amounts of a different slab component than in mBAB-N. Their Ba/Yb and Th/Yb relative to Nb/Yb ratios are intermediate between those of AMW and QVF, their Ba/Th ratios are as high as at the QVF (>230), and their $^{143}Nd/^{144}Nd$ are slightly lower than in AMW relative to Nb/Yb. Ce/Pb ratios are lower, Ba/La ratios are higher, and $^{207}Pb/^{204}Pb$ and $^{208}Pb/^{204}Pb$ isotope ratios are higher relative to $^{206}Pb/^{204}Pb$ and overlap QVF at >18.70. $^{87}Sr/^{86}Sr$ ratios also are up to 0.0006 higher relative to $^{143}Nd/^{144}Nd$ than in AMW and mBAB-N (Fig. 6). Defined this way, basalts from the Ngatoro Rift at 36.2°S, the Ngatoroirangi Rift at 33.5°, and some from the Rumble V Ridge and adjacent Rift are mBAB-S (Wright et al., 1996; Wysoczanzki et al., 2010; Todd et al., 2010, 2011). Volatile contents have been measured in some glasses and two melt inclusions from the Ngatoroirangi Rift (Wysozcanzki et al., 2010). All are degassed, but H_2O contents are 1.5-2.5 wt% nevertheless.

4.3 Reararc (RA)

We refer to active and inactive volcanoes that are located west of the Quaternary volcanic front and have more arc-like geochemistry than mBAB but differ geochemically from QVF, as "reararc" (RA). Those north of the Central Kermadec Discontinuity (RA-N) are <40 km behind the QVF, lie between the QVF and mBAB geographically, and are from relatively shallow seamounts (<1500 mbsl) at the east end of indistinct cross-arc ridges. Indeed, two RA-N are active volcanoes that sometimes are included in "the Kermadec Arc": Giggenbach and Havre. The RA seamounts to the south of the Central Kermadec Discontinuity (RA-S) extend the full width of the Havre Trough, are from <3000 mbsl which is shallower than mBAB-S in this area, and are more similar to QVF geochemically than are RA-N.

4.3.1 Reararc north of the Central Kermadec Discontinuity (RA-N)

We sampled near the two large active RA-N volcanoes: Giggenbach (DR55-58, 117) behind Macauley Island; and Havre (DR123, 124) behind L'Esperance Rock. We also found RA-N dacites to rhyolites at seamounts a similar distance behind Raoul (DR106, 107), and RA-N lavas were found previously behind Curtis Island (SO135-42DR: Haase et al., 2002).

RA-N and QVF samples differ geochemically in several ways. First, RA-N basalts are medium-K, the only such in the Havre Trough, and strongly tholeiitic (Fig. 3). They have lower SiO_2 than QVF, especially relative to FeO*/MgO. Second, the enrichment in K_2O also characterizes other incompatible elements like LREE (Fig. 4), as is true for reararc magmas globally. The most consistent exceptions are Ba and Pb, contributing to shallower slopes for Ba/Yb versus Nb/Yb (Fig. 4), lower Ba/La ratios (<30) (Fig. 5), and higher Ce/Pb ratios (5-10 for RA versus <5 for QVF). Third, the shallower slopes in Nb/Yb diagrams partly reflect greater Nb-enrichment than in QVF. This is most clearly seen relative to Nd isotopes (Fig. 6). Fourth, as with mBAB-N, REE patterns for RA-N basalts are steeper than for QVF, even within the HREE (i.e., Dy/Yb_N > 1.1: Fig. 5), and have similar S-shaped REE patterns as northern BAB and mBAB. Fifth, the enrichment in LREE is greater than for Zr-Hf, resulting in large negative Hf concentration anomalies (Sm/Hf > 1.7) even at 6-7 wt% MgO (Fig. 5b). Finally, they have lower $^{87}Sr/^{86}Sr$ relative to $^{143}Nd/^{144}Nd$ ratios than QVF (Fig. 6).

Many of these differences between RA-N and QVF also separate older rocks from the Colville and Kermadec Ridges that were, respectively, the reararc versus volcanic front of the Vitiaz Arc prior to opening of the Havre Trough (Hoernle et al., In Rev.). RA-N differ from mBAB-N by having greater enrichment in slab-related characteristics (e.g. higher K_2O; higher Ba/Yb, La/Yb and Th/Yb at a given Nb/Yb; higher Sm/Hf at a given Zr/Hf; lower Ce/Pb and higher Ba/La: Fig. 3a, 4a-c, 5b-c), and by including more differentiated and calcalkaline rocks.

4.3.2 Reararc south of the Central Kermadec Discontinuity (RA-S)

RA-S lie behind QVF volcanoes south of 32°S and clearly differ from mBAB-S geochemically, but they are less different from QVF than are RA-N. Therefore, it appears that QVF-like magmas extend across the full width of the Havre Trough south of the Central Kermadec Discontinuity. This was first discovered at 36°S where the Rumble V Ridge extends almost to the Colville Ridge (Gamble et al., 1996; Todd et al., 2010), and at isolated seamounts including Gill volcano in the west, adjacent seamounts on the westernmost Kibblewhite Ridge (Rapuhia, Yokosuka, and Giljanes), the eastern Ngatoro Rift wall, and the Rumble2-West seamount in the east (Wright et al., 2006; Wysoczanski

et al., 2010; Todd et al., 2011; Timm et al., 2016). We added 39 samples from 17 sites. In general, RA-S compositions characterize rocks from seamounts and ridges shallower than 3000 mbsl (except DR149 from the side of the deep NW-trending basin behind Haungaroa), whereas BAB-S basalts come from deeper basins (except DR20 from Kibblewhite Ridge). Apart from the Rumble V Ridge, the most continuous RA-S edifices constitute what we call Kibblewhite Ridge and sampled at DR19-25.

Most RA-S differ from RA-N by being low-K and having a wider range of SiO_2 (Fig. 3) The most calcalkaline RA-S are atypical high-Mg andesites (SiO_2=58%; Mg#=57) in DR24 and 25 from the sides of a >2500 m-deep basin immediately north of the Kibblewhite main cone.

Although most RA-S have greater enrichment in slab-related trace elements than mBAB-S, most also have lower (La,Th,Ba)/Yb with respect to Nb/Yb ratios than QVF or most RA-N, resulting in shallower slopes on Nb/Yb diagrams (Fig. 4). Indeed, a few RA-S with Nb/Yb=0.9-3.5 lie within the AMW field for La/Yb, and are similar to mBAB for Th/Yb. They are clearly from quite fertile AMW mantle, so that only the most incompatible slab-related elements such as Ba, Pb, and U show relative enrichments. RA-S span the widest range of mantle and slab trace element enrichments in the Havre Trough, from mBAB to QVF values, but usually with less Pb and U enrichment than in QVF (i.e., higher Ce/Pb (Fig. 8) and higher Nb/U ratios, not shown). Their REE patterns overlap those of the more enriched QVF, and most lack the distinctive steeper HREE and large negative Hf anomalies of most RA-N. Because the REE patterns of RA-S are flatter, they cross the patterns of RA-N in the middle REE (Fig. 5d). The high-Mg andesites near Kibblewhite have the most U-shaped HREE patterns (not shown).

The amount and character of slab component in RA-S makes it more difficult to assess the nature of its mantle component, but RA-S (except for Gill volcano) have higher Hf isotope ratios than RA-N, just as Hf isotope ratios in mBAB-S are higher than in mBAB-N (Fig. 6). However, the literature data identified as RA in Fig. 6 are mostly for RA-S and show a wide range of $^{176}Hf/^{177}Hf$ ratios that Todd et al. (2011) attributed to heterogeneity within the AMW. Both RA types have $^{143}Nd/^{144}Nd < 0.51305$, and most are well below AMW values for their Nb/Yb and $^{176}Hf/^{177}Hf$ ratios (Fig. 6). Relative to Nb/Yb, Th-enrichment is greatest when $^{143}Nd/^{144}Nd$ is lowest, and least when

$^{143}Nd/^{144}Nd$ is near AMW values. That is, relative enrichment in Th concentrations and Nd isotope ratios is least in RA-S samples from the most Nb-rich mantle (e.g., DR23 and SIO-41D-A (Todd et al., 2011), behind Kibblewhite). Most RA-S have similar enrichment in $^{87}Sr/^{86}Sr$ relative to $^{143}Nd/^{144}Nd$ as in QVF. Pb isotopes in RA-S also overlap QVF values and extend to more radiogenic values than in RA-N and mBAB-S.

Basalts from Gill volcano in the western Havre Trough have the most enriched Nd-Hf isotopes, almost the most radiogenic Sr, and the greatest La and Th enrichment of all RA samples, approaching the most enriched values for the southern volcanic front. However, it has the lowest $^{87}Sr/^{86}Sr$ ratios relative to $^{143}Nd/^{144}Nd$, so that it lies along the RA-N trend. Our two samples from the deep southeastern flank are even more enriched in Sr-Nd isotope and La/Yb ratios than those from the northern mid-flank reported by Todd et al. (2011). Nevertheless, ours have only half the Nb-Ta contents and even more negative Hf concentration anomalies, demonstrating larger intra-volcano variability in HFSE than observed closer to the volcanic front. The same variability characterizes the reararc seamount chains behind the Izu arc where it was attributed to the heterogeneous mantle sources of a single volcano (Machida et al., 2008).

4.4 Colville Ridge Horsts (CRH)

Samples from two of our Havre Trough sites, DR7 and DR154, have distinctive Pb isotope ratios, with $^{208}Pb/^{204}Pb$ but not $^{207}Pb/^{204}Pb$ above the QVF field (Fig. 7). This unique feature characterizes 3-8 Ma samples from both halves of the older Vitiaz Arc -- the Kermadec and Colville Ridges (Hoernle et al., In Rev.). Sites DR7 and DR154 lie 20-30 km east of the Colville Ridge on what look like down-dropped horsts in the high-resolution bathymetry of Tontini et al. (2019, Fig. 2a) and Hoernle et al. (2017). Samples from both sites have 1-2 cm-thick Mn crusts. Our samples do not have the lowest $^{206}Pb/^{204}Pb$ or greatest LREE-enrichment of the most distinctive Colville Ridge rocks, but they share some of the geochemical features including low TiO_2 relative to MgO, Ce/Pb <5, and low $^{143}Nd/^{144}Nd$ relative to $^{176}Hf/^{177}Hf$ than QVF. Although they are undated and more mafic than most Colville Ridge samples, we consider them possible candidates to be foundered Vitiaz Arc crust, the first to be discovered in the Havre Trough, albeit not

far "in". Both lie near or directly above what was interpreted previously as spread crust formed ~5 Ma (Tontini et al., 2019).

4.5 Rhyolites derived from mBAB north of the Central Kermadec Discontinuity (mBAB-NR)

We discovered a previously undescribed 900 m-high circular caldera in the middle of the Havre Trough at ~30°S, near the west end of a discontinuous NW-trending ridge that extends ~65 km behind Macauley. The caldera is 2 km-wide and 400 m-deep (Fig. 9). We sampled its outer flank at DR115 at 1250-1550 mbsl, its inner walls at similar depth at DR111 and 112, and a satellite cone on its eastern rim at 1100-1500 mbsl (DR116). All rocks are alkali feldspar-phyric, glassy, vesicular lava, not pumice. The K-feldspar in DR112-1 is 52.4 ±9.6 ka, providing the highest precision evidence of very youthful volcanism in the middle of the Havre Trough.

Fig. 9

All of our 13 samples are highly differentiated alkali rhyolite with ~0.1 wt% MgO and <0.7% CaO. They have 6.5-7.7 wt% Na_2O, 2.7-3.5 % K_2O, and straddle the pantellerite-comendite boundary of MacDonald (1974). They are completely different geochemically from the low-K rhyolites at the QVF like those from Macauley for which we report data for comparison (Table S1).

The extent of differentiation is extreme; e.g., Th contents are 20 times higher in the rhyolite than in nearby mBAB-N basalt. Therefore, the volume of basaltic parental melt at this site would overwhelm the crust. However, the rhyolites have high Ce/Pb ratios and are isotopically the same as mBAB-N from the nearby DR113 (Figs. 6-8) apart from having slightly higher $^{206}Pb/^{204}Pb$ ratios. That is, the rhyolites have minimal components from either the pre-existing arc or the slab, and could be derived from mBAB-N-type basalt from a high Nb/Yb source. Some trace element ratios in the rhyolites are affected by the differentiation. For example, Nb/Yb and Th/Yb ratios are 2 to 3 times higher, respectively, in the rhyolite than the basalt, yet even they still lie within the MORB array with values at the high end of E-MORB (Fig. 4). The most notable differences from mBAB-N basalts are the development of large negative Sr and Eu concentration anomalies, large positive Zr and Hf anomalies, and flatter HREE in the

rhyolites. These characteristics presumably reflect extensive fractionation of feldspar and pyroxene.

Both the backarc location and rhyolitic composition of the caldera lavas are similar to those at Mayor Island, a morphologically young volcano just north of New Zealand within the southernmost extension of the Havre Trough (Ewart et al., 1968; Cole, 1978). Mayor Island rhyolites are somewhat more pantelleritic, more potassic, less sodic, and generally more "continental" in trace element and isotope ratios. Nevertheless, the two volcanoes are the only current examples of alkali rhyolite in an active intra-oceanic backarc basin.

4.6 Quaternary Volcanic Front (QVF)

Thirty-three mostly submarine volcanoes define the Kermadec Quaternary Volcanic Front (QVF), all but seven of which are known to be active at least hydrothermally (de Ronde et al., 2007). The geochemistry of their lavas has been studied extensively (e.g., Gamble et al., 1990; Wright et al., 2006). Our 40 samples come from near the northernmost QVF volcanoes in the Havre Trough – Kibblewhite, Cole, Kuiwai, and Haungaroa -- plus rhyolites from Macauley caldera, and basalts to andesites from DR64 further north between Hinetapeka and Putoto.

Most Kermadec QVF lavas, including most of our basalts to andesites, have low-K, tholeiitic compositions by the criteria of Gill (1981) (Fig. 3), and are very Nb-depleted (Nb/Yb < 0.4, less than even most D-MORB). They form linear arrays with steep slopes on Nb/Yb vs. Ba/Yb, La/Yb, and Th/Yb diagrams (Fig. 4). Their relative enrichment is less for La than Ba and Th, and most QVF basalts have sub-chondritic La/Sm ratios. Their HREE patterns are as flat as in MORB (Fig. 5a). The greatest enrichment relative to HREE, especially in Th and Ba, is in medium-K Kibblewhite basalts from DR28. This kind of diversity at Kibblewhite was known before but only for the tallest seamount, the site of our DR26 (Wright et al., 2006; Timm et al., 2014). Zr/Hf ratios are 30-40 which is lower (more depleted) than in most BAB (Fig. 5b). The only samples with negative Hf concentration anomalies (i.e., Sm/Hf >1.7) are the most LREE-enriched ones in DR28. Ce/Pb and Nb/U ratios are low (<7 and <5, respectively), whereas Ba/La is high (>30) as in most arcs (Fig. 5c).

[143]Nd/[144]Nd ratios in our QVF samples range from 0.51290 to 0.51305, and are lower than in ambient mantle relative to their Nb/Yb and [176]Hf/[177]Hf ratios (Fig. 6). This displacement relative to Hf isotopes also is true for Tonga (Pearce et al., 2007; Hergt and Woodhead, 2007), and differs from the initial claim for Kermadec (Woodhead et al., 2001). Both Nd and Hf isotope ratios are lowest in the high-K lavas from Clark Volcano at the southernmost volcanic front (Gamble et al., 1996).

Our [87]Sr/[86]Sr ratios lie within the range of literature values for QVF rocks (Fig. 6). They range from ~0.7040 in the more typical low-K rocks down to ~0.7035 in the medium-K, more Nb-enriched lavas at Kibblewhite. The latter are uncommon for the Kermadec volcanic front but fill a gap amongst literature data for similarly unradiogenic Sr at both higher and lower [143]Nd/[144]Nd. The highest [87]Sr/[86]Sr values in the QVF are in the south, at Clark and RumbleII-East seamounts.

Pb isotope ratios in the QVF appear to be dominated by the kind of sediment found in the Kermadec Trench and derived from New Zealand (Fig. 7). Our double-spiked Pb isotope ratios are tightly correlated with [206]Pb/[204]Pb ratios between 18.65-18.95. The less radiogenic end would intersect the NHRL and AMW values at ~18.4. The more radiogenic end approaches trench sediment. Our data agree with other spiked results (see Fig. 6 caption for references), and confirm that the least radiogenic Pb is in the north at Macauley.

All isotope ratios for our QVF lavas, and for literature values, become more enriched on average (i.e., more like Kermadec trench sediment) southward toward New Zealand. Most of these overall geochemical features, and their latitudinal dependence, are shared with the youngest rocks of the Kermadec Ridge that was the volcanic front >1 Ma. They differ geochemically from older rocks of the Kermadec Ridge by lacking EM1-type Pb and Sr isotope ratios (Hoernle et al., In Rev.).

4.6. Summary

The geochemical diversity of Havre Trough volcanic rocks has spatial pattern. BAB have little or no subduction component, extend the previously known range of the AMW, and are more depleted south of the Central Kermadec Discontinuity. They are most like EPR N-MORB and basalts from the Central Lau Spreading Center elementally,

and are unlike the isotopically "Indian" basalts of the Central and East Lau Spreading Centers that are unknown south of 23°S. Their Nb/Yb ratios correlate negatively with ^{143}Nd/^{144}Nd and ^{176}Hf/^{177}Hf as in MORB. mBAB have a small amount of slab component, but less than even in most of the East Lau Spreading Center.

RA basalts come from shallower seamounts and contain more slab component than mBAB that mostly occupy deeper basins. In general, RA lie closer to the volcanic front than mBAB. (La,Th,Ba)/Yb ratios are elevated above AMW and MORB values relative to Nb/Yb in both RA and mBAB, but more so in RA. Relative to ^{143}Nd/^{144}Nd, ^{87}Sr/^{86}Sr ratios are displaced above AMW-trend values in both mBAB-S and most RA-S but not in mBAB-N or RA-N. RA lavas have lower ^{143}Nd/^{144}Nd than mBAB, especially relative to Nb/Yb and ^{176}Hf/^{177}Hf.

RA and mBAB from north of the Central Kermadec Discontinuity come from more enriched mantle, with mostly higher Nb/Yb and lower ^{143}Nd/^{144}Nd and ^{176}Hf/^{177}Hf ratios than mBAB-S and RA-S. However, the northern slab component is less enriched in fluid-mobile elements. mBAB-N and RA-N have less radiogenic Sr and Pb, higher Ce/Pb, and lower Ba/La ratios. mBAB-N has greater Ti-enrichment during differentiation than mBAB-S. We will argue below that the slab component is more melt-like in the north and more fluid-like in the south.

This summary infers that different slab components were introduced into different mantle sources in ways that vary consistently along and across the strike of the Havre Trough. Although mBAB and RA melt compositions *could* be created by mixing BAB and QVF melts, as inferred for mBAB-type basalts at ODP Site 834 in the older Lau Basin (Hergt and Nilsson-Farley, 1994), we consider this an unlikely explanation of our intermediate basalt types because they were erupted scores of km behind the volcanic front, further than magma is known to travel away from the front of modern arcs.

5 Discussion

5.1 The Havre Trough Ambient Mantle Wedge (AMW)

We introduced the concept of Ambient Mantle Wedge in Section 2 to refer to what the mantle wedge composition was like before addition of a subduction component. It was first applied to the SW Pacific by Todd et al. (2010). It ranges from being more

depleted than DMM to more enriched, and is best sampled by what we call BAB. Our four new BAB sites join three others in the Havre Trough and three from spread crust in the adjacent and wider South Fiji Basin (DSDP Sites 205 and 285, and Alison Seamount) (Mortimer et al., 2007; Pearce et al., 2007; Todd et al., 2011). The AMW defined in this way underlay the Vitiaz Arc system since its inception (Todd et al., 2012).

The SW Pacific AMW is surprisingly similar to sources of East Pacific Rise MORB in trace element and isotope ratios (Figs. 4-8). That similarity is surprising because, first, so much of it is no more depleted than N-MORB in Nb/Yb and other trace element ratios that are little affected by a slab component, especially north of the Central Kermadec Discontinuity. In contrast, the AMW for the arc (both the modern QVF and older Kermadec Ridge) was uniformly more depleted than even D-MORB. Nb/Yb ratios in much of the Havre Trough already are as high as in the Mariana Trough which is up to ~200 km wide and has been actively spreading for several million years (Pearce et al., 2005). Nb/Yb ratios are higher than along the Central and East Lau Spreading Centers (e.g., Bezos et al., 2009). Therefore, the AMW during the rifting stage is at least as fertile as during the spreading stage, and already has replaced the more depleted mantle from when the arc was active.

Somewhat less surprising is that the AMW is like the EPR mantle isotopically. It remains "Pacific"-like rather than the "Indian"-like asthenospheric mantle that replaced it beneath the Lau and North Fiji Basins after seafloor spreading separated the frontal and remnant parts of the Vitiaz Arc there (Pearce et al., 2007). The southern-most extent of the new Indian-like mantle is ~23°S. However, a striking dissimilarity between the AMW and EPR MORB is that AMW has lower $^{143}Nd/^{144}Nd$ relative to Nb/Yb ratios or vice versa (Fig. 6), and most of its $^{206}Pb/^{204}Pb$ ratios are 18.7-18.8 even when Ce/Pb = 15-28 (Fig. 8). That is, although it extends to even greater Nb-depletion than in DMORB, it is like N- to E-MORB isotopically. As a result, the $^{206}Pb/^{204}Pb$ of most of the AMW sources of Havre Trough basalts (with three exceptions) is similar to that of trench sediment, resulting in a nearly vertical mixing array in $^{206}Pb/^{204}Pb$ versus Ce/Pb (Fig. 8a). This Nb-depletion yet isotopic enrichment of the AMW characterized the Vitiaz Arc system throughout its history (Gill, 1984; Todd et al., 2012)

The wide range of Nb/Yb ratios (0.1 to 3.5) in tholeiitic basalts minimally affected by slab-derived enrichments means that basalts related to backarc rifting preserve a wider range of mantle depletion to enrichment than basalts related to spreading. Presumably this reflects less mixing than during magma focusing at spreading centers. AMW is most uniformly depleted at the QVF, less depleted for RA, and least depleted and most variable for BAB and mBAB-N. The positive correlation between Nb/Yb and Zr/Hf suggests the same pattern. The negative correlation between Nb/Yb and $^{143}Nd/^{144}Nd$ means that much of the depletion reflects their coupled relationship within the AMW such that preferential melting of Nb-rich and ^{143}Nd-poor "plums" leaves a depleted mantle residue in the backarc (see Pearce, 2005). The triangular mixing pattern between Nb/Yb and Ce/Pb (Fig. 8b) reflects flux-melting in which the addition of more water-rich and Pb-rich flux results in more melting of variably depleted mantle.

BAB, mBAB, and RA are all more depleted in Nb and Nd-Hf isotopes south of the Central Kermadec Discontinuity, even though pockets of enriched mantle remain (e.g., DR23 in the eastern Havre Trough, and OIB-like basalts on the west side of the southern Colville Ridge: Timm et al., 2019; Hoernle et al., In Rev..). A possible explanation for this greater depletion may be some kind of tectonic inheritance. The Central Kermadec Discontinuity may be the eastward continuation of a boundary between the northern versus southern South Fiji Basin. A complicated case can be made that backarc basin spreading behind the Eocene Vanuatu-Fiji-Lau-Tonga-Kermadec arc substrate, that we refer to as the Vitiaz Arc, created only the northern half of the South Fiji Basin (the Minerva Abyssal Plain) (Herzer et al., 2011; Bassett et al., 2016). In contrast, these authors argue that the southern half of the South Fiji Basin (the Kupe Abyssal Plain) formed by spreading within and south of a feature called the Julia Extensional Transform Zone or East Julia Zone due to rollback of the Pacific Plate along the northern edge of Zealandia without any pre-existing arc above the subducting plate. It was backarc spreading behind no arc! If so, then there is no pre-Miocene arc crust or mantle lithosphere south of the Central Kermadec Discontinuity. For some reason, this kind of spreading seems to have left more depleted mantle in its wake, to be inherited by the more usual kind of backarc extension that has now commenced in the Havre Trough. In addition, we will argue below that the subduction component south of the Central

Kermadec Discontinuity was more water-rich, which may result in larger degrees of mantle flux-melting and, therefore, more depleted basalts.

5.2 Nature and amount of the slab components

The slab component that characterizes the Kermadec QVF has been well documented for decades (e.g., Gamble et al., 1990; Ewart et al., 1998; Wright et al., 2006). Most QVF basalts and andesites are low-K; enriched in $^{87}Sr/^{86}Sr$, Ba, Th, U, and to a lesser extent LREE, relative to Yb; and enriched in Pb relative to Ce. Nb/Yb ratios, TiO_2, and Na_2O contents are lower relative to MgO than in most BAB. This coupled depletion in HFSE but enrichment in fluid-mobile elements usually is attributed to more flux melting of the mantle beneath the QVF than beneath the backarc. This is consistent with QVF rocks having more radiogenic Pb and Sr relative to $^{143}Nd/^{144}Nd$, but also lower $^{143}Nd/^{144}Nd$ relative to Nb/Yb and $^{176}Hf/^{177}Hf$. Those traits usually are attributed to a slab component that is a hydrous melt or super-critical fluid derived from sediment ± altered basaltic ocean crust, which is consistent with water-saturated melting at the predicted local slab surface temperature (Syracuse et al., 2010). Whether or not the source of the slab melt includes basaltic crust, much less how enriched such crust is (e.g., Castillo et al., 2009), or exactly how fluid-like the melt is, matters primarily at the volcanic front and is beyond the scope of this paper.

Our QVF samples are representative in these respects, and similar to the <3 Ma rocks of the older Kermadec Ridge, the previous arc front (Hoernle et al., In Rev.). Because Nd isotope ratios are lower relative to Hf isotope ratios in the QVF than in the AMW, and Sm/Hf ratios are generally higher (Figs. 5,6), the slab melt may be partly derived from subducted sediment and leave residual zircon (Todd et al., 2011). Both the mass fraction of slab component and the extent of source depletion increase to the south, especially where the QVF steps westward into the Havre Trough. This may reflect more flux melting, greater prior mantle depletion, or both, there.

RA-N come from 15-40 km behind the QVF and differ geochemically from the QVF in ways that are characteristic of reararc volcanoes worldwide. mBAB-N are even farther behind the QVF and intermediate between RA-N and BAB geochemically. Therefore, we infer that they have a smaller mass fraction of a similar slab component.

Many differences between mBAB and RA north versus south of the Central Kermadec Discontinuity reflect addition of a larger mass fraction of a slab component in the south, or its addition to a more depleted mantle, or both. However, the nature of the slab component seems different too. The northern slab component results in more Fe+Ti-enrichment during differentiation of mBAB, and has lower Ba/La, higher Ce/Pb, lower $^{87}Sr/^{86}Sr$ ratios relative to $^{143}Nd/^{144}Nd$, and Pb isotopes below the QVF trend in mBAB-N. Therefore, we consider this slab component to be higher-temperature, drier, and more melt-like. For illustrative purposes, we model it using a slab component that is 80% sediment melt and 20% super-critical fluid at 6 GPA and 800°C. (See Todd et al., 2011, Table 4 for details; we assumed 20% batch melting of trench sediment with <0.6% residual rutile>zircon, and added the slab component to DMM mantle pre-depleted by removal of 0.6% melt). Our new model results are shown as open red circles in Figures 4 and 6. Most mBAB-N require only ≤0.006% of such a melt-rich component to explain their trace element and isotope ratios. In contrast, samples from near the large RA-N volcanoes require 3-4 times more of the melt-like slab component. Partial melts of a modified mantle are shown as red x's. If the degree of mantle melting is ~10%, then Nb/Yb ratios increase less than two-fold in the melt so that most of the variability in that ratio reflects the mantle source. However, some of the compositional scatter for RA probably reflects smaller melt fractions, and variable initial enrichment, of the modified mantle. More slab melt in the north may also explain the steeper HREE in both mBAB and RA there.

In contrast, the slab component in the south seems to be wetter because it is richer in slab-derived Sr, Pb, Ba, and U, and generally is more similar to slab components at the QVF. Illustrative model results are shown in Figures 4 and 6 as open blue circles, assuming the same conditions as used by Todd et al. (2011) for mBAB-S basalts from the Ngatoroirangi Rift where the slab component is entirely a super-critical fluid. mBAB-S require 0.1-0.4% of this more dilute component, whereas RA-S require up to 1% followed by smaller degrees of mantle melting shown as blue x's, down to 2-4% for the Kibblewhite high-Mg andesites and <2% for Gill volcano. Because about a third of RA-S basalts have 20-50% negative Hf concentration anomalies, slab surface temperatures must often be low enough for melts to remain saturated in zircon (Todd et al., 2011).

The preceding discussion uses the models of Todd et al. (2011) for consistency and convenience, but they are merely illustrative and depend on many assumptions. However, the general difference between a drier and more melt-like slab component added to a more enriched mantle in the north, versus a more fluid-like slab component added to a more depleted mantle in the south, is necessary to explain the regional geochemical differences. Because a more water-rich slab component will promote higher degrees of mantle melting, the two explanations are additive. The general west-to-east gradation from mBAB to RA to QVF in the north, and the general difference between mBAB-rich basins versus RA-rich ridges in the south, mean that an even more granular model such as proposed by Todd et al. (2011) probably is needed. At minimum, we infer a wide range of fluid/melt properties in the RA-S slab component to produce the fan-shaped array of Sr-Nd isotopes from QVF to RA-N. However, even our large number of analyzed samples is insufficient to constrain a more detailed model for the entire Havre Trough now.

The variation in amount and kind of slab component between basalt types is similar to the pattern observed along the Rumble V Ridge (Todd et al., 2010), and between "rift-type" versus "arc-type" basalts elsewhere in the Havre Trough (Todd et al., 2011). Todd et al. (2011) calculated that what we call mBAB basalts contain <0.3% slab component based on their trace element and isotope ratios, whereas what we call RA-S have 0.3-1.0%. Our results are broadly similar.

Several geochemical aspects of BAB and mBAB basalts are similar to those of basalts from rifts behind the Izu volcanic front (Hochstaedter et al., 2001). Those features reflect a distinctive combination of the extent of prior mantle depletion, the depth and degree of mantle melting, and the nature and amount of the slab component. In Izu, the S-shaped REE pattern in particular has been shown to indicate 2-4% melting at ~1.5 GPa of mantle more depleted than DMM to which ~0.5% of hydrous melt was added from a slab 120-140 km deep (Miyazaki et al., 2020). We infer variations on this theme along and across the strike of the Havre Trough, and suggest that the S-shaped REE patterns may characterize the rifting stage of backarc development in general because they seem to be absent from the spreading stage of the Lau Basin and Mariana Trough.

It is unclear why the slab component would become generally wetter towards the south. Slab surface temperatures beneath the arc are expected to increase gradually southward (Syracuse et al., 2010). Consequently, although about half the subducted water is predicted to be exhaled beneath the Havre Trough under equilibrium conditions, the maximum water flux is expected to be shallower in the south (van Keken et al., 2011). Perhaps there is more bend faulting in the south approaching the Hikurangi Plateau beneath which such faulting is thought to result in extensive hydration of the subducting crust and mantle (Herath et al., 2020). Another explanation might be an anomalously steep slab dip north of the Central Kermadec Discontinuity. We noted in Section 2 that the slab appears to steepen between 28° and 32°S, with a large cluster of intermediate depth earthquakes (200-450 km) beneath the western Havre Trough at ~30°S (e.g., Hayes et al., 2018). This might focus more slab melt beneath the Havre Trough.

Some of our samples from Kibblewhite are atypically enriched in K and Nb, and enriched in LREE relative to Hf, yet have less radiogenic Pb, lower $^{87}Sr/^{86}Sr$ relative to $^{143}Nd/^{144}Nd$, and even lower $^{143}Nd/^{144}Nd$ relative to $^{176}Hf/^{177}Hf$. This may reflect a hotter slab surface and more melt-like slab component beneath Kibblewhite Ridge similar to what was proposed for the Rumble V Ridge by Todd et al. (2011).

5.3 Spatial distribution of the slab components within the Havre Trough

Arc-like basalts and andesites have been known to occur within the southern Havre Trough for decades (e.g., Gamble et al., 1995; Wright et al., 1996). The most dramatic example is the Rumble V Ridge along which what we refer to as RA-S and mBAB-S basalts are interspersed from the arc front almost to the Colville Ridge remnant arc. In general, RA-S (called XAM by Todd et al., 2010) are most common near the front, and mBAB-S are more common closer to the remnant arc, but the progression is irregular and the most extreme RA-S is in the far west. All are <0.7 Ma (Wysoczanzki et al., 2019). Subsequent work found "arc-type" rocks mostly on shallower seamounts, and "rift-type" rocks in deeper basins such as the Ngatoroirangi Rift whose floor was sampled using a submersible (Wysoczanski et al., 2010; Todd et al., 2011). This led to speculation that slab components in the Havre Trough might be focused in rerarc seamount chains like those in the Izu arc and result from "hot fingers" of the kind inferred for NE Japan

(Tamura et al., 2002). The concept is that regularly spaced cells of hotter than usual mantle develop along strike within the mantle wedge at a high angle to the arc, preferentially melt the underlying slab, and result in seamount chains that are enriched in a slab-melt component. Subsequent numerical modeling found conditions in which this might occur (Kim and Lee, 2018).

Although we found variable amounts and kinds of slab components throughout the Havre Trough north of 35°S, there is no equivalent of the Rumble V Ridge, much less regular spacings thereof. The closest match is what we call the Kibblewhite Ridge ~150 km north of Rumble V Ridge, but it differs in two important respects. First, it is less distinct morphologically, and it is parallel to the NE-trending seafloor fabric whereas the Rumble V Ridge cuts across it. Second, there seems to be less slab component in the Kibblewhite Ridge, because its Sr-Nd-Pb isotopes are less enriched. This contrast is most evident relative to Nb/Yb ratios.

We did find short ridge-like coalesced RA seamounts behind QVF volcanoes north of the Central Kermadec Discontinuity. There, the amount of slab component decreases with increasing water depth and distance from the QVF along a ridge behind L'Esperance, from RA-N at DR123 near Havre, to mBAB-N at DR118-122 and P63474. Except for DR118, the dredge depth deepens in that same sequence. BAB (SO135-41DR: Haase et al., 2002) was dredged from a basin just north of this ridge and almost as close to the QVF as the RA-N DR123. This is consistent with a decreasing mass fraction of melt-like slab component with increasing distance behind the QVF, and with focusing of the slab component at a high angle to the arc, leaving the adjacent AMW less affected.

It may be that the robust long seamount chains in the Izu reararc reflect something unique to their structural setting, or to a certain time interval during arc evolution. They pre-date the current phase of rifting in Izu, and cannot be traced across its ~100 km-wide extensional zone to connect to arc front volcanoes. They did not develop until several million years after "rift-type" volcanism (Sato et al., 2020; Miyazaki et al., 2020). Therefore, the messy spatial distribution of slab components in the Havre Trough may have a temporal dimension as well, and be commonplace during rifting and prior to spreading.

Similar geochemical complexity applies to volcanism in the northernmost Mariana Trough where spreading gives way to rifting yet a "spreading axis" has been identified at the eastern margin of the Trough closest to the Mariana volcanic front (Stern et al., 1990; Alt et al., 1993; Martinez et al., 1995; Gribble et al., 1998; Pearce et al., 2005; Woodhead et al., 2012). Based on older data for fewer samples, BAB as defined in Section 4.1 of this paper is present in the northern Mariana Trough only where the spreading axis is >150 km behind the volcanic front. Basalts are mBAB-type to within 120 km of the volcanic front (the "Central Graben" area), and become even more arc-like (RA-type) as they draw closer to the arc in the Southern Volcano Tectonic Zone where they are joined by the Kasuga reararc seamount chain of RA-type shoshonitic basalts (Stern et al., 1993; Fryer et al., 1997). If the Mariana Trough is un-zipping south to north, then the Havre Trough can be thought of as torn fabric of about the same width but four times the length and with geochemically similar basalts at similar distance behind its volcanic front throughout.

In summary, we did not find convincing evidence of multiple "hot fingers" (Tamura et al., 2005) of reararc seamount chains in addition to the one described at 36°S by Todd et al. (2011). We did find an alignment of seamounts with mostly RA-S compositions at what we called Kibblewhite Ridge at 34.5°S, and suggestive ridges are present north of the CKD where RA-N is restricted to <40 km behind the QVF. We found that the percent of slab component increases southward in the Havre Trough just as in the QVF. We also found that seamounts in the eastern half of the Havre Trough are *not* consistently "characterized by an island arc basalt composition which might possibly record the migration from proto-Colville-Kermadec arc to the present active volcanic front" (Tontini et al., 2019).

5.4 Geochemical comparison of "Rifting" and "Spreading" in backarc basins

As backarc rifting evolves into spreading, the stress field changes, the mantle dehydrates and strengthens, and eventually organized vertical upwelling and spreading ensue (Lin et al., 2010; Magni, 2019). We noted in Section 5.1 that the previous sub-arc

mantle is replaced even during the rifting stage, and that replenishment is by mantle at least as fertile (measured by Nb/Yb ratios) as during active spreading.

In addition, there is a different distribution of slab components in the rifting and spreading stages. This is shown by two examples in the Lau Basin where backarc spreading centers propagate toward the Tongan volcanic front. The Eastern Lau Spreading Center is ~100 km behind the front at 20°S, but only 40 km behind it at 22.5°S (Valu Fa) (Taylor et al., 1996). Its volcanic rocks become more arc-like southward (Martinez et al., 2006; Bezos et al., 2009; Escrig et al., 2009). In the north they are like basalts from the Central Lau Spreading Center that are minimally affected by a slab component and that we call BAB. Even ~60 km behind the volcanic front, the slab component is at most like our mBAB-S. Not until Valu Fa, where the ridge becomes inflated and the lavas become andesitic, do compositions approach our RA-S. Even Pb isotopes never quite overlap ratios of the Tongan volcanic front; they are always displaced toward Indian AMW.

A similar pattern occurs at the Fonualei Spreading Center (FSC) further north (Keller et al., 2008; Caulfield et al. 2012; Escrig et al., 2012). Its northern end is ~75 km behind the Tongan volcanic front whereas the southern end is only 25 km behind it. The AMW at the FSC is more enriched (e.g., Nb/Yb=0.8-1.5) but the pattern is the same: less slab component in the north, and progressively more to the south, although the pattern appears less regular at the FSC. Ba, Th, and to a lesser extent La are enriched relative to Yb and Nb all along the FSC, but by only as much as in Havre Trough mBAB in the north, and never by as much as Havre Trough RA in the south. Ce/Pb is only 5-10 in the north, and decreases southward. Sr isotopes never reach the values of the Tongan volcanic front (they are like our mBAB-N), and even Pb isotopes are like those of the Tongan front only within 40 km behind it.

Trace element ratios along the Mariana Trough spreading centers are known with less spatial resolution but for greater distance (Pearce et al., 2005; Woodhead et al., 2012). Basalts from the Southern Mariana Trough (13-18°N) >70 km from the volcanic front are like our BAB. Most of those from the central Mariana Trough (16-20°N), that are up to 150 km behind the volcanic front, are like our mBAB. All of these are considered to be from "spreading" centers. Only some from what are considered "rifting"

areas are like our RA basalts, as noted in Section 5.3. Nb/Yb ratios have a similar range in both the Mariana Trough and Havre Trough. Therefore, much of the mantle beneath the Havre Trough already is as replenished by similarly fertile mantle and as little affected by slab components as along the actively spreading Mariana Trough. In detail, our mBAB-N have what Pearce et al. (2005) refer as their Ba-Th deep subduction component, whereas our mBAB-S also have what Pearce et al. (2005) refer as their Ba-only shallow subduction component that is restricted to the volcanic front in the Marianas. The difference between their deep and shallow components is what we call melt-rich versus fluid-rich that we distinguish more by temperature than depth of origin.

Therefore, during spreading, a small amount of melt-like slab component (as in our mBAB-N) is distributed throughout the backarc up to 150 km behind the volcanic front, but significant amounts (like our RA) stay within 40 km of the volcanic front, and the distribution of the slab component is more regular than during rifting. The Tongan examples are surprising because the subduction angle there is shallower than in the Havre Trough, and the slab is shallower beneath the QVF. Both might be expected to spread the slab component farther into the backarc.

During Havre Trough rifting, significant amounts of melt-like slab component (our RA) also remain within 15-40 km of the volcanic front north of the Central Kermadec Discontinuity but extend up to 100 km behind it in the south, sometimes but not always in seamount chains. Small amounts of slab component (i.e., BAB and mBAB) feed volcanism >40 km behind the volcanic front in both cases, but also characterize basalts, usually in deeper basins, that are interspersed with RA to within 20 km of the front. The spatial pattern is much more random than during spreading.

The differences between rifting and spreading may reflect easier lateral transport and mixing of magma along the strike of spreading centers, or a difference in the flow pattern and style of deformation of the mantle as it dehydrates and the basin widens. Either or both will affect transport of the slab component as rifting evolves toward spreading. As a result, the rifting stage is more disorganized geochemically as well as spatially.

5.5. Whatever happened to the Vitiaz Arc?

Remnants of the pre-existing Vitiaz Arc appear to be largely absent from the surface of the ocean floor of the Havre Trough, in contrast to what was predicted by Katz (1978). Although somewhat QVF-like rocks are present south of the Central Kermadec Discontinuity (i.e., our RA-S type), they differ geochemically from rocks from the Kermadec and Colville Ridges, and they are ≤1 Ma old (Wysoczanski et al., 2019). The unusual isotopic character of the Vitiaz Arc from 3-7 Ma (Hoernle et al., In Rev..) should make its remnants easy to spot, but at most only two of our 165 samples qualify: namely, the CRH samples from within 30 km of the Colville Ridge. Although Havre Trough crust is thicker than normal oceanic crust, and has a more arc-like velocity structure, any remaining Vitiaz Arc crust is well hidden, and has had too little effect on magma rising through it to erase the spatial pattern of Havre Trough basalts noted above. Even when a large volume of basalt is present within the crust beneath the rhyolite caldera, the differentiates are closely related to sources in the mantle, not the Vitiaz Arc crust.

This means that even "disorganized arc rifting" (Wysoczanksi et al., 2010) involves extreme and rapid attenuation of arc crust prior to spreading. It is uncertain when rifting started but arc volcanism as young as 2.6 Ma is known on the Colville Ridge south of the Central Kermadec Discontinuity (Timm et al., 2019). Rifting may have started shortly before or afterwards.

5.6. Mantle flow during the rifting stage, and the role of backarc basin formation in arc evolution

An important uncertainty in all arcs and backarcs is how to distinguish recent slab components from ancient mantle enrichments resulting from previous slab components. It is often inferred that the mantle beneath the reararc is less depleted than beneath the arc front whereas the slab component beneath the reararc is more depleted in fluid-mobile elements because of up-dip dehydration (e.g., Hochstaedter et al., 2001). We infer from the range of Nb/Yb and Nd-Hf-Pb isotope ratios in BAB and mBAB-N samples that a wide range of mantle depletion and enrichment already is present in the Havre Trough AMW. Those trace element and isotopic characteristics extend to OIB-like values (Nb/Yb ~45; $^{206}Pb/^{204}Pb$ ~19.3) in seamounts of the South Fiji Basin (Mortimer et al.,

2007; Todd et al., 2011) and the Colville Ridge (Timm et al., 2019; Hoernle et al., In Rev.). Therefore, in this section we focus on the BAB and mBAB in which there is little evidence of even LREE being added from the slab to the mantle wedge. At most, slab-derived Pb, Sr, Ba, U, ±Th are present in them, reflecting addition of <0.4% of slab fluid (Todd et al., 2011).

We find it remarkable that such basalts are so widespread during the rifting versus spreading stage of backarc evolution. They are found for >700 km along the Havre Trough which is longer than the spreading centers of the Lau Basin and at least ¾ the length of the Mariana Trough. Their Nb/Yb ratios are as high as in the Mariana Trough. Most are from 50-70 km behind the volcanic front, but some are within 20 km of it. Therefore, well before arc crust is thinned or replaced beyond seismic recognition, and before spreading starts, the mantle wedge can be purged of most of the slab-affected material that fed the Vitiaz Arc prior to rifting, and it is replenished by relatively un-depleted asthenospheric mantle. This change is most dramatic in the removal of the distinctive EM1-enriched-type material that affected both the Kermadec and Colville Ridges at 3-7 Ma (Hoernle et al., In Rev.), but even the ordinary slab component of the ridges is more dilute in the backarc and the ambient mantle is less depleted, especially north of the Central Kermadec Discontinuity.

The Izu arc is another example where new mantle with minimal slab component appears within 20 km of the volcanic front during the rifting stage of backarc basin development (e.g., Hochstaedter et al., 1990; Gill et al., 1992; Hirai et al., 2018). Basalts in these rifts are <1.5 Ma, and are like our BAB or mBAB even though the crustal thickness exceeds that of the Havre Trough.

The same is true in the Lau Basin. The oldest basalts of its rifting stage are like our BAB or mBAB in their trace element and isotope ratios. They are from the >3 Ma igneous basement of ODP Site 834 located ~100 km east of the Lau Ridge remnant arc (Parson and Hawkins, 1994; Hergt and Nilsson-Farley, 1994). Although the older slab component was already mostly gone, the AMW remained "Pacific" isotopically, and was not yet replaced by new "Indian" mantle. The latter did not appear until spreading started. Like Havre Trough mBAB, the least arc-like Site 834 basalts have S-shaped REE patterns. They are more like E-MORB than N-MORB in their $^{206}Pb/^{204}Pb$ ratios even

when Ce/Pb ratios are >20, and even the most arc-like lavas have Ce/Pb ratios >10, far above those of the Tongan volcanic front.

This cycle of mantle depletion during arc activity versus re-fertilization during backarc opening may play an important role in the overall evolution of arc crust. Similar secular changes in Nb/Yb and Hf isotope ratios have been attributed to fluctuations between arc magmatism and backarc basin formation in the Izu-Mariana arc system (e.g., Gill et al., 1994; Bryant et al., 2003; Straub et al., 2015; Brandl et al., 2017), and in exhumed arc crust in Kohistan (Jagoutz et al., 2018).

In summary, the ~100 km of separation between the Kermadec and Colville Ridges does not just reflect crustal attenuation and commensurate upwelling of the mantle that previously underlay it. Instead it reflects rapid advection of new mantle into the wedge. The most depleted new mantle, with the lowest Nb/Yb and highest ^{143}Nd/^{144}Nd and ^{176}Hf/^{177}Hf, occurs at 32° to 33.5°S, within the Central Kermadec Discontinuity, just south of where the Vitiaz Arc may end (Bassett et al., 2016). The rapid disappearance of slab-contaminated mantle from beneath an arc seems to be a common phenomenon. Depletion and rapid re-fertilization of the mantle wedge modulates arc crustal evolution.

6 Conclusions

The Ambient Mantle Wedge (AMW) beneath the Havre Trough remains "Pacific"-type during the rifting stage of backarc development, unlike the more "Indian"-type beneath the Lau Basin during its spreading stage. Basalts are more elementally and isotopically enriched, like N- to E-MORB, north of the Central Kermadec Discontinuity (CKD) at 32°S than south of it. The greater depletion of basalts in the south may reflect a more depleted source inherited from the South Fiji Basin, or a higher degree of flux-melting as a result of a wetter slab component, or both.

We present the first complete trace element and multi-isotope analyses for the three northernmost active arc front volcanoes that lie within the Havre Trough (Cole, Kuiwai, and Haungaroa), and we assign two other active volcanoes (Havre and Giggenbach) to reararc status. Magmas from the frontal volcanoes come from a mantle

more depleted than the D-MORB source, and contain a slab-derived component that is dominated by trench sediment.

Basalts in the rest of the Havre Trough range from having almost no subduction influence (BAB), to slight (mBAB), to significant at rear arc volcanoes (RA). The slab component is drier and more melt-like north of the Central Kermadec Discontinuity, and more like fluid or wet melt to the south. The mass fraction of slab component increases southward in the Havre Trough just as in the QVF.

Only two examples of possible stranded horsts of the pre-existing Vitiaz Arc were found at the surface of the Havre Trough, both within 30 km of the remnant Colville Ridge. Little geochemical evidence of contamination by pre-existing crust was found even where large volumes of basalt invaded the crust and differentiated to alkali rhyolite at a newly-documented 56 ka caldera in the middle of the basin.

Mantle that previously underlay the Vitiaz Arc seems to be largely absent beneath the Havre Trough soon after rifting started. It has been replaced by less depleted, more fertile mantle that extends the full width of the Havre Trough. Such rapid mantle replenishment may modulate the arc crustal evolution.

During the rifting stage of backarc development, significant mass fractions of slab component can extend further into the backarc, and be absent closer to the volcanic front, than when spreading occurs. Overall, the slab component is distributed in a less systematic fashion than during the spreading stage. That is, the rifting stage is more disorganized geochemically as well as spatially.

Acknowledgements

References

Alt, J.C., W. Shanks, and M.C. Jackson (1993) Cycling of sulfur in subduction zones: Mariana Island Arc and back-arc trough, *Earth Planet. Sci. Lett.* 119, 477-494.

Barker, S. J., C. J. N. Wilson, J. A. Baker, M.-A. Millet, M. D. Rotella, I. C. Wright, and R. J. Wysoczanski (2013) Geochemistry and Petrogenesis of Silicic Magmas in the Intra-Oceanic Kermadec Arc. *J. Petrology* 54(2), 351–391.

Bassett D., H. Kopp, R. Sutherland, S. Henrys, A. Watts, C. Timm, M. Scherwath, I. Grevenmeyer, and C. De Ronde (2016) Crustal structure of the Kermadec Arc from MANGO seismic refraction profiles, *J. Geophys. Res.* 121, 7514-7546. Doi:10.1002/2016JB013194.

Bezos, A., S. Escrig, C.H. Langmuir, P.J. Michael, and P.D. Asimow (2009) Origins of chemical diversity of back-arc basin basalts: a segment-scale study of the Eastern Lau Spreading Center, *J. Geophys. Res.* 114, B06212, doi:10/1029/2008JB005924.

Brandl, P.A., M. Hamada, R.J. Arculus, K. Johnson, K.M. Marsaglia, I.P. Savov, O. Ishizuka, and H. Li (2017) The arc arises: The links between volcanic output, arc evolution and melt composition. *Earth Sci. Rev.* 461, 73-84.

Bryant, C., R. J. Arculus, and S. M. Eggins (2003) The geochemical evolution of the Izu-Bonin arc system: A perspective from tephras recovered by deep-sea drilling. *Geochem. Geophys. Geosystems* 4(11), 1094.

Castillo P.R., P.F. Lonsdale, C.L.Moran, and J.W. Hawkins (2009) Geochemistry of mid-Cretaceous Pacific crust being subducted along the Tonga-Kermadec Trench: implications for the genmeration of arc lavas. Lithos 112, 87-102.

Caulfield J., S. Turner, R. Arculus, C. Dale, F. Jenner. J. Pearce, C. Macpherson, and H. Handley (2012) Mantle flow, volatiles, slab-surface temperatures and melting dynamics in the north Tonga arc-Lau back-arc basin. *J. Geophys. Res.* 117, B11209, doi:10.1029/2012JB009526.

Class, C., and K. Lehnert (2012) *PetDB Expert MORB (Mid-Ocean Ridge Basalt) Compilation, Version 1.0.* Interdisciplinary Earth Data Alliance (IEDA). doi:10.1594/IEDA/100060. Accessed 2020-06-27.

Cole, J. (1978) Tectonic setting of Mayor Island volcano. *N.Z. Journal Geol. Geophys.* 21, 645-647.

Coleman P.J. and G.H. Packham (1976) The Melanesian borderlands and India-Pacific plates' boundary. *Earth Sci. Rev.* 12,197-233.

Collot, J-Y. and B. Davy (1998) Forearc structures and tectonic regimes at the oblique subduction zone between the Hikurangi Plateau and the southern Kermadec margin. *J. Geophys. Res.* 103, 623-650.

DeMets C., R.G. Gordon, D.F. Argus, and S. Stein (1994) Effects of recent revisions to the geomagnetic resersal time scale on estimates of current plate motions. *Geophy. Res. Lett.* 21, 2192-2194.

de Ronde, C., E.T. Baker, G.J. Massoth, et al., (2007) Submarine hydrothermal activity along the mid-Kermadec arc, New Zealand: large-scale effects of venting, *Geochem. Geophys. Geosystems* 8(7) Q07007, doi:10.1029/2006GC001495.

Escrig, S., A. Bezos, S.L. Goldstein, C.H. Langmuir, and P.J. Michael (2009) Mantle source variations beneath the Eastern Lau Spreading Center and the nature of subduction components in the Lau basin-Tonga arc system, *Geochem. Geophys. Geosystems* 10(6) Q0414, doi:10.1029/2008GC002281.

Escrig, S., A. Bézos, C. H. Langmuir, P. J. Michael, and R. J. Arculus (2012) Characterizing the effect of mantle source, subduction input and melting in the Fonualei Spreading Center, Lau Basin: Constraints on the origin of the boninitic signature of the back-arc lavas, *Geochem. Geophys. Geosystems* 13, Q10008.

Ewart A., K.D. Collerson, M. Regelous, J.I. Wendt, and Y. Niu (1998) Geochemical evolution within the Tonga-Kermadec Lau arc back-arc systems: the role of varying mantle wedge composition in space and time, *J. Petrol.* 39, 331-368. Doi:10.1093/petrology/39.3.331.

Ewart A,, S.R. Taylor, and A.C. Capp (1968) Geochemistry of the pantellerites of Mayor Island, New Zealand, Contr. Mineral. and Petrol. 17, 116-140.

Fryer P., J.B. Gill, and M.C. Jackson (1997) Volcanologic and tectonic evolution of the Kasuga seamounts, northern Mariana Trough: ALVIN submersible investigations. *J. Volc. Geothermal Res.* 79, 277-311.

Fujiwara T., T. Yamazaki, and M. Joshima (2001) Bathymetry and magnetic anomalies in the Havre Trough and southern Lau Basin: from rifting to spreading in back-arc basins. *Earth Planet. Sci. Lett.*185, 253-264.

Gamble, J.A., I.E.M Smith, I.J. Graham, B.P Kokelaar, J.W. Cole, B.F. Houghton, and C.J.N. Wilson (1990) The petrology, phase relations, and tectonic setting of basalts from the Taupo volcanic zone and the Kermadec island arc-Havre Trough, SW Pacific. *J. Volcanol. Geothermal Res.* 43, 253-270.

Gamble, J.A., J.D. Woodhead, I. Wright, and I. Smith (1996) Basalt and sediment geochemistry and magma petrogenesis in a transect from oceanic island arc to rifted continental margin arc, SW Pacific (1996) *J. Petrology* 37, 1523-1546.

Gamble, J.A., I.C. Wright, J.D. Woodhead, and M.T. McCulloch (1995) Arc and backarc geochemistry in the southern Kermadec arc-Ngatoro Basin and offshore Taupo Volcanic Zone, SW Pacific, in *Volcanism Associated With Extensional Consuming Plate Margins* ed. J.L. Smellie, *Geol. Soc. Spec, Pub*. 81, 193-212.

Gill, J. (1976) Composition and age of Lau Basin and Ridge volcanic rocks: implications for evolution of an interarc basin and remnant arc, *Geol. Soc. Amer. Bull*. 87, 1384-1393.

Gill J. (1981) *Orogenic Andesite and Plate Tectonics*. Spring-Verlag 390pp.

Gill, J. (1984) Sr-Pb-Nd isotopic evidence that both MORB and OIB sources contribute to oceanic island arc magmas in Fiji. *Earth Planet. Sci. Letters* 68, 443-458.

Gill, J. and M. Gorton (1973) A proposed geological and geochemical history of eastern Melanesia in *The Western Pacific: Island arcs, marginal seas, geochemistry.* ed P. Coleman, Western Australia University Press 543-566.

Gill J., R.N. Hiscott, and Ph. Vidal (1994) Turbidite geochemistry and evolution of the Izu-Bonin arc and continents. *Lithos* 33, 135-168.

Gill J., C. Seales, P. Thompson, A. Hochstaedter, and C. Dunlap (1992) Petrology and geochemistry of Plioecen-Pleistocene volcanic rocks from the Izu Arc In*: Proc. ODP Sci. Results* 126, 627-651.

Gribble, R.F., R.J. Stern, S. Newman, S. Bloomer, and T. O'Hearn (1998) Chemical and isotopic composition of lavas from the Northern Mariana Trough: implications for magma genesis in back-arc basins, *J. Petrol.* 39, 125-154.

Haase, K., T.J. Worthington, P. Stoffers, D. Garbe-Schoenberg, and I. Wright (2002) Mantle dynamics, element recycling, and magma genesis beneath the Kermadec Arc-

Havre Trough, *Geochem. Geophys. Geosystems* 3(11) 1071,
doi:10/1029/2002GC000335.

Hauff, F., Hoernle, K., Gill, J., Werner, R., Timm, C., Garbe-Schönberg, D., Gutjahr, M.,
Jung, S. (2020) R/V SONNE Cruise SO255 "VITIAZ": An integrated major element,
trace element and Sr-Nd-Pb-Hf isotope data set of volcanic rocks from the Colville and
Kermadec Ridges, the Quaternary Kermadec volcanic front and the Havre Trough
backarc basin, Version 1.0. Interdisciplinary Earth Data Alliance
(IEDA). doi:10.26022/IEDA/111723. Accessed 2020-10-28.

Hayes, G.P., G. Moore, D. Portner, M. Hearne, H. Flamme, M. Furtney, and G. Smoczyk
(2018) Slab2, a comprehensive subduction zone geometry model, *Science*
10.1126/science.aat4723.

Herath P., T.A. Stern, M.K. Savage, D. Bassett, S. Henrys, and C. Boulton (2020)
Hydration of the crust and upper mantle of the Hikurangi Plateau as it subducts at the
southern Hikurangi margin. *Earth Planet. Sci. Lett.* 541, 116271.

Hergt J.M and K. Nilsson-Farley (1994) Major element, trace element, and isotopes (Pb,
Sr, and Nd) variations in Site 834 basalts: implications for the initiation of backarc
opening. *In* Hawkins, J, Parson L., Allan J. et al. *Proc. ODP Sci. Results,* 135: College
Station TX (Ocean Drilling Program) 471-485.

Hergt J.M. and J.D.Woodhead (2007) A critical evaluation of recent models for Lau-
Tonga arc-backarc basin magmatic evolution. *Chem. Geol.* 245, 9-44.

Herzer R.H., D.H.N. Barker, W.R. Roest, and N. Mortimet (2011) Oligocene-Miocene
spreading history of the northern South Fiji Basin and implications for the evolution of
the New Zealand plate boundary. *Geochem. Geophys. Geosystems. 12(2)
Q02004,*doi:10.1029/0GC003291.

Heywood, L.J., S. M. DeBari, J.B. Gill, S.M.Straub, J.C. Schindlbeck-Belo, R. Escobar-Buricaga, and J.D. Woodhead (2020) Across-arc diversity in rhyolites from an intra-oceanic arc: evidence from IODP Site U1437, Izu-Bonin rear-arc and surrounding area, *Geochem. Geophys. Geosystems.* 21, e2019GC008353. doi:10.1029/2019GC008353

Hirai, Y., T. Yoshida. S. Okamura, Y. Tamura, I. Sakamoto, and R. Shinjo (2018) Breakdown of residual zircon in the Izu arc subducting slab during backarc rifting, *Geology* 46(4), 371-374.

Hochstaedter, A., J.B. Gill, and Morris J.D. (1990) Volcanism in the Sumisu Rift II: subduction and non-subduction related components. *Earth Planet. Sci. Lett.* 100, 195-209.

Hochstaedter, A., J.B. Gill, R. Peters, B. Broughton, P. Holden, and B. Taylor (2001) Across-arc geochemical trends in the Izu-Bonin arc: contributions from the suducting slab, *Geochem. Geophys. Geosystems.* 2(7) 1019, doi:10.1029/2000GC0000105.

Hoernle, K., F. Hauff, P. van der Bogaard, R. Werner, N. Mortimer, J. Geldmacher, D. Garbe-Schönberg, and B. Davy (2010) Age and geochemistry of volcanic rocks from the Hikurangi and Manihiki oceanic plateaus. *Geochim. Cosmochim. Acta* 74, 7196-7219.

Hoernle, K., F. Hauff, and R. Werner (2017) RV SONNE Fahrbricht/Cruise Report SO255: VITIAZ – The Life Cycle of the Vitiaz-Kermadec Arc/Backarc System: from arc initiation to splitting and backarc basin formation. Auckland (New Zealand) - Auckland (New Zealand) 02.03-14.04.2017.

Hoernle, K., C. Timm, J. Gill, F. Hauff, R. Werner, and D. Garbe-Schonberg (In Review) Geochemistry of Kermadec and Colville Ridges, SW Pacific: Did plateau/fracture zone subductioon trigger Vitiaz Arc breakup? *Geology*

Honda, S., T. Yoshida, and K. Aoike (2007) Spatial and temporal evolution of arc volcanism in the northeast Honshu and Izu-Bonin arcs: evidence of small-scale convection under the island arc? *Island Arc* 16, 214-223.

Ishizuka O., R.N. Taylor, A.A. Milton, and R.W. Nesbitt (2003) Fluid-mantle interaction in an intra-oceanic arc: constraints from high-precision Pb isotopes. *Earth Planet. Sci. Lett*. 211, 221-236.

Jagoutz O., P. Bouilhol, U. Schaltegger, and O. Müntener (2019) The isotopic evolution of the Kohistan Ladakh arc from subduction initiation to continent arc collision. In: Treloar P.J. and Seale M.P. (eds) Himalayan Tectonics: a modern synthesis. Geological Society London Spec. Pub. 483. Doi.org/10.1144/SP483.7.

Karig, D.E. (1970) Ridges and basins of Tonga-Kermadec island arc system, *J. Geophys. Res*. 75, 239-254, doi:10.1029/JB075i002p00239.

Katz, H.R. (1978) Composition and age of Lau Basin and Ridge volcanic rocks: Discussion. *Geol. Soc. Amer. Bull*. 89, 1118-1120.

Keller, N.S., R.J. Arculus, J. Hermann, and S. Richards (2008) Submarine back-arc lava with arc signature: Fonualei Spreading Center, northeast Lau Basin, Tonga, *J. Geophys. Res.* 113, B08S07 doi:10.1029/2007JB005451.

Kim, Y-M and C. Lee (2018) Mantle temperature anomaly in southern Kermadec speculated by three-dimensional numerical subduction modeling, *Geo-Marine Lett*. 38, 351-358.

Lin, S-C., B-Y. Kuo, and S-L. Chiung (2010) Thermomechanical models for the dynamics and melting processes in the Mariana subduction system, *J. Geophys. Res*. 115, B12403, doi:10.1029/2010JB007658.

MacDonald, R. (1974) Tectonic setting and magma associations. *Bull. Volcanol.* 38, 575-593.

Machida, S., T. Ishii, J.I. Kimura, S. Awaji, and Y. Kato (2008) Petrology and geochemistry of cross☐chains in the Izu☐Bonin back arc: Three mantle components with contributions of hydrous liquids from a deeply subducted slab. *Geochem. Geophys. Geosystems* 9(5).

Magni, V. (2019) The effects of back-arc spreading on arc magmatism, *Earth Planet. Sci. Lett.* 519, 141-151.

Malahoff, A., R. Foden, and H. Fleming (1982) Magnetic anomalies and tectonic fabric of marginal basins north of New Zealand, *J. Geophys. Res. 87,* 4109-4125.

Martin, A.K. (2013) Double-saloon-door tectonics in the North Fiji Basin, *Earth Planet. Sci. Lett.* 374, 191-203.

Martinez, F., P. Fryer, N. Baker, and T. Yamazaki (1995) Evolution of backarc rifting: Mariana Trough, 20°-24°N, *J. Geophys. Res.* 100, 3807-3817.

Martinez, F. and B. Taylor (2006) Modes of crustal accretion in back-arc basins: inferences from the Lau Basin. in *Back-Arc Spreading Systems: Geological, Biological, Chemical, and Physical Interactions* eds. D.M. Christie, C.R. Fisher, S-M. Lee, S. Givens, *Geophysical Mon.* 166. AGU.

Martinez, F., B. Taylor, E.T. Baker, J.A. Resing, and S.L. Walker (2006) Opposing trends in crustal thickness and spreading rate along the back-arc Eastern Lau Spreading Center: implications for controls on ridge morphology, faulting, ands hydrothermal activity, *Earth Planet. Sci. Lett.* 245, 655-672.

McDonough W.F. and S.S. Sun (1995) The composition of the earth. *Chem. Geol.* 120, 223-253.

Miyashiro A. (1974) Volcanic rock series in island arcs and active continental margins. *Am. J. Sci, 274*, 321-355.

Miyazaki, T., J. B. Gill, C. Hamelin, S. M. DeBari, T. Sato, Y. Tamura, J□I. Kimura, B.S. Vaglarov, Q. Chang, R. Senda, and S. Haraguchi (2020) The First 10 Million Years of Rear□Arc Magmas Following Backarc Basin Formation Behind the Izu Arc. *Geochem. Geophys. Geosystems* 21, e2020GC009114.

Mortimer N., R.H. Herzer, P.B. Gans, C. Laporte-Magoni, A.T. Calvert, and D. Bosch (2007) Oligocene-Miocene tectonic evolution of the South Fiji Basin and Northland Plateau, SW Pacific: evidence from petrology and dating of dredged rocks. *Marine Geology* 237, 1-24.

Mortimer N., P. van den Bogard, K. Hoernle, C. Timm, P.B. Gans, R. Werner, and F. Riefstahl (2019) Late Cretaceous oceanic plate reorganization in the Pacific-Zealandia region. *Gondwana Res.* 65, 31-42.

Niu, Y., K.D. Collerson, R. Batiza, J.L. Wendt, and M. Regelous (1999) Origin of enriched-type mid-ocean ridge basalt at ridges far from mantle plumes: The East Pacific Rise at 11°20'N, *J. Geophys. Res.*, 104, 7067-7087, doi:10/1029/1998JB900037.

Niu, Y., D. Waggoner, J. Sinton, and J. Mahoney (1996) Mantle source heterogeneity and melting processes beneath seafloor spreading centers: The East Pacific Rise, 18°-19°S. *J. Geophys. Res.*, 101, 27,711-27,733. Doi:10.1029/96JB01923.

Parson, L.M. and J.W Hawkins (1994) Two-stage ridge propagation and the geological history of the Lau backarc basin. *In* Hawkins, J, Parson L., Allan J. et al. *Proc. ODP Sci. Results,* 135: College Station TX (Ocean Drilling Program) 819-828.

Pearce, J.A. (2005) Mantle preconditioning by melt extraction during flow: theory and petrogenetic implications. *J. Petrology* 46, 973-997.

Pearce, J.A., P.D. Kempton, and J.B. Gill (2007) Hf-Nd evidence for the origin and distribution of mantle domains in the SW Pacific, *Earth Planet. Sci. Lett.* 260, 98-114, doi:10.1016/j.epsl.2007.05.023.

Pearce, J.A., R.J. Stern, S.H. Bloomer, and P. Fryer (2005) Geochemical mapping of the Mariana arc-basin system: implications for the nature and distribution of subduction components. *Geochem. Geophys. Geocystems* 6(7) Q07006, doi:10.1029/2004GC000895

Price R.C., N. Mortimer, I.E.M. Smith, and R. Maas (2015) Whole-rock geochemical reference data for Torlesse and Waipapa terraces, North Island, New Zealand. *N.Z. Journal Geol. Geophys.* 58, 213-228.

Reyners M, D. Eberhart-Phillips, and S. Bannister (2011) Tracking repeated subduction of the Hikurangi Plateau beneath New Zealand. *Earth Planet. Sci. Lett.* 311, 165-171.

Salters V.J.M., S. Mallick, S.R. Hart, C.H. Langmuir, and A. Stracke (2011) Domains of depleted mantle: new evidence from hafnium and neodymium isotopes. *Geochem. Geophys. Geosystems* 12(8) Q08001 doi:10.1029/2011GC003617.

Sato, T., T. Miyazaki, Y. Tamura, J. Gill, M. Jutzeler, R. Senda, and J-I Kimura (2020) The earliest stage of Izu rear arc volcanism revealed by drilling to Site U1437, IODP Expedition 350, *Island Arc* doi: 10.1111/iar.12340, 1-18.

Sinton, J. and P. Fryer (1987) Mariana Trough lavas from 18°N: implications for the origin of back arc basin basalts, *J. Geophys. Res.* 92, 12782-12802.

Stern, R.J., P. Lin, J. Morris, M.C. Jackson, P. Fryer, S. Bloomer, and R. Ito (1990) Enriched back-arc basin basalts from the northern Mariana Trough: implications for the magmatic evolution of back-arc basins, *Earth Planet. Sci. Lett.* 100, 210-225.

Stern R.J., M.C. Jackson, P. Fryer., and E. Ito (1993) O, Sr, Nd, and Pb isotopic composition of the Kasuga Cross-Chain in the Mariana Arc: a new perspective on the K-h relationship. *Earth Planet. Sci. Lett.*119, 459-475.

Straub, S. M., J. D. Woodhead, and R. J. Arculus (2015) Temporal Evolution of the Mariana Arc: Mantle Wedge and Subducted Slab Controls Revealed with a Tephra Perspective. *J. Petrology* 56(2), 409–439.

Syracuse, E.M., P.E. van Keken, and G.A. Abers (2010) The global range of subduction zone thermal models. *Physics Earth Planet. Int.* 183, 73-90.

Tamura, Y., Y.Tatsumi, D. Zhao, Y. Kido, and H. Shukuno (2002) Hot fingers in the mantle wedge: new insights into magma genesis in subduction zones. *Earth Planet. Sci. Lett*. 197, 105–116.

Taylor B., K. Zellmer, F. Martinez, and A. Goodlife (1996) Sea-floor spreading in the Lau backarc basin, *Earth Planet. Sci. Lett*. 144, 35-40.

Timm, C., B. Davy, K. Haase, K.A. Hoernle et al. (2014) Subduction of the oceanic Hikurangi Plateau and its impact on the Kermadec arc. *Nature Communications* 5:2923, doi:10.1038/ncomms5923.

Timm, C., M.I. Leybourne, K. Hoernle, R.J. Wysoczanski, F. Hauff, M. Handler, F.C. Tontini, and C. de Ronde (2016) Trench-perpendicular geochemical variation between two adjacent Kermadec Arc volcanoes Rumble two East and West: the role of the subducted Hikurangi Plateau in element recycling in arc magmas. *J. Petrology* 57, 1335-1360.

Timm, C., C. de Ronde, K.A. Hoernle, B. Cousens, J-A. Wartho, F.C. Tontini, R. Wysoczanski, F. Hauff., and M. Handler (2019) New age and geochemical data from the southern Colville and Kermadec Ridges, SW Pacific: insights into the recent geological history and petrogenesis of the Proto-Kermadec (Vitiaz) arc. *Gondwana Res.* 72, 169-193, doi:10.1016/gr.2019.02.008.

Todd E., J.B. Gill, and J.A. Pearce (2012) A variably enriched mantle wedge and contrasting melt types during arc stages following subduction initiation in Fiji and Tonga, SW Pacific. *Earth Planet. Sci. Lett.* 335-336, 180-194.

Todd E., J.B. Gill, R.J. Wysoczanski, M.R. Handler, I.C.Wright, and J.A. Gamble (2010) Sources of constructional volcanism in the southern Havre Trough: new insights from HFSE and REE concentration and isotope systematics. *Geochem. Geophys. Geosystems* 11, Q04009.

Todd E., J.B. Gill, Wysoczanski, J. Hergt, I.C.Wright, M.I. Leybourne, and N. Mortimer (2011) Hf isotopic evidence for small-scale heterogeneity in the mode of mantle wedge enrichment: souther Havre Trough and South Fiji Basin back-arcs. *Geochem. Geophys. Geosystems* 11, Q09011.

Tontini, F.C., D. Bassett, C. de Ronde, C. Timm., and R. Wysoczanski (2019) Early evolution of a young back-arc basin in the Havre Trough, *Nature Geoscience* 12, 856-864.

van Keken, P. E., B. R. Hacker, E. M. Syracuse, and G. A. Abers (2011) Subduction factory: 4. Depth-dependent flux of H_2O from subducting slabs worldwide, *J. Geophys. Res.* 116(B1), B01401.

van de Lagemaat, S., D. van Hinsbergen, L. Boschman, P. Kamp, and W. Spakman (2018) Southwest Pacific absolute plate kinematic reconstruction reveals major Cenozoic Tonga-Kermadec slab dragging, *Tectonics* 37, 2647-2674.

Woodhead J.D., J.M. Hergt, J.P Davidson, and S.M. Eggins (2001) Hafnium isotope evidence for 'conservative' element mobility during subduction zone processes. *Earth Planet. Sci. Lett.* 192, 331-346.

Woodhead J.D., R.J. Stern, J. Pearce, J.M. Hergt, and J. Vervoort (2012) Hf-Nd isotope variation in Mariana Trough basalts: the importance of "ambient mantle" in the interpretation of subduction zone magmas *Geology* 40, 539-542,

Wright, I.C., L.M. Parson, and J.A. Gamble (1996) Evolution and interaction of migrating cross-arc volcanism and back-arc rifting: an example from the southern Havre Trough (35°20'-37°S). *J. Geophys. Res.* 101, 22071-22086.

Wright, I.C., T.J. Worthington, and J.A. Gamble (2006) New multi-beam mapping and geochemistry of the 30°S-35°S seafloor, and overview of southern Kermadec arc volcanism. *J. Volcanol Geothermal Res.* 149, 263-296.

Wysoczanski, R., G. Leonard, J. Gill, I. Wright, A. Calvert, W. McIntosh, B. Jicha, J. Gamble, C. Timm, M. Handler, E. Drewes-Todd, and A. Zohrab (2019) Ar-Ar age constraints on the timing of Havre Trough opening and magmatism. *N.Z. Journal Geol. Geophys.* 62, 371-377, doi:10.1080/00288306.2019.1602059.

Wysoczanski R., E. Todd, I.C. Wright, M.I. Leybourne, J.M. Hergt, C. Adam, and K. Mackay (2010) Backarc rifting, constructional volcanism, and nascent disorganized spreading in the southern Havre Trough backarc rifts (SW Pacific). *J. Volcanol Geothermal Res.* 190, 39-57.

Wysoczanski, R., I. Wright, J. Gamble, E.H. Hauri, J.F. Luhr, S.M. Eggins, and M. Handler (2006) Volatile contents of Kermadec Arc-Havre Trough pillow glasses: fingerprinting slab-derived aqueous fluids in the mantle sources of arc and back-arc lavas. *J. Volcanol Geothermal Res.* 152, 51-73.

Yang, S., M. Humayun, and V. Salters (2020) Elemental constraints on the amount or recycled crust in the generation of mid-ocean ridge basalts (MORBs). *Sci. Adv*. 6, eaba2923.

Figure Captions

Figure 1. Regional bathymetric map showing features discussed in the text. The rectangle shows the location of Figure 2. ELSC, Eastern and Central Lau Spreading Centers; FSC, Fonualei Spreading Center. Base map is from "The GEBCO_2014 Grid, version 20150318, http://www.gebco.net".

Figure 2. Area of this study showing the locations of dredge (DR) stations for all the samples in Table 1. Symbols for those stations identify their most common rock type, are identified in the legend, and are used in subsequent figures. See text for explanation of symbol acronyms. The yellow stars are dredge sites from the literature and referred to in the text. The white dashed line shows the Quaternary Volcanic Front (QVF). Note that it lies within the eastern Havre Trough south of 31°3 S, but lies on the Kermadec Ridge further north. The solid white line labeled CKD shows the location of the Central Kermadec Discontinuity. QVF volcanoes are identified by letters in black squares as follows, from south to north: He, Healy; B, Brothers; Ki, Kibblewhite; S, Sonne; N, Ngatoroirangi; C, Cole; Ku, Kuiwai; Hu, Huanharoa; W, Wright; L'E, L'Esperance; Ha, Havre; V, Volcanolog; Cu, Curtis; M, Macauley; G, Giggenbach; R, Raoul; Hi, Hinetapeka; P, Putoto. The base map is from "The GEBCO_2014 Grid, version 20150318, http://www.gebco.net".

Figure 3. (a) SiO_2 vs. K_2O. The lines separate the Low-K, Medium-K, and High-K boundaries of Gill (1981). Note that most QVF, BAB, and mBAB are low-K, whereas most RA-N are medium-K. (b) SiO_2 vs. FeO^*/MgO where FeO^* is total Fe as FeO. The line shows the boundary between calcalkaline and tholeiitic from Miyashiro (1974). The steep vertical trend at 49-52% SiO_2 in RA-N is tholeiitic. The only strongly calcalkaline rocks are RA-S high-Mg andesites (HMA) from DR24+25 adjacent to Kibblewhite. Rhyolites are omitted. (c) MgO-TiO_2. Note that BAB is like MORB, mBAB-N has only slightly lower TiO_2 relative to MgO, and the rest have significantly less, presumably reflecting increasingly early magnetite saturation and, therefore, higher fO_2. A few samples with higher and lower MgO are omitted in order to emphasize the rest. MORB data in this and other figures are from the EPR: Niu et al. (1996, 1999), Class and Lehnert (2012), and Yang et al. (2020).

Figure 4. Nb/Yb vs. Ba/Yb (a), La/Yb (b), and Th/Yb (c). Displacement along the EPR MORB trend reflects relative depletion to enrichment of the mantle. Displacement above the MORB trend reflects addition of a slab component to the mantle wedge source. Depending on the element ratio, BAB representing the Ambient Mantle Wedge (AMW) lie within or just above the MORB field. Therefore, they have little or no slab component. The other rock types have more. Mixing models in red for north of the Central Kermadec Discontinuity, and in blue for south, are based on models in Todd et al. (2011). See text for model assumptions. Open stars near the origin show the assumed ambient mantle compositions that are relatively less depleted north of the Central Kermadec Discontinuity (AMWE = DMM minus 0.4% melt), and more depleted south (AMWD = DMM minus 0.6% melt). Open circles show mixtures of AMW plus a slab component (slab melt for the northern component, slab fluid for the southern one) in 20 mass fraction increments of 0.0002 ending at 0.004. X's show batch melts of the modified mantle that contains 0.0016 slab component in the north and 0.0010 in the south. Numbers >1 identified by dashed lines give the percent melting, and show the relatively small effect of <10% melting on Nb/Yb ratios. The source of literature (Lit.) data, and their assignment to BAB, mBAB, RA, and QVF categories are given in the text. Samples with Nb/Ta <10 are omitted because of potential Nb-Ta contamination. The D, N, and E-

MORB are from the EPR (Niu et al., 1996, 1999; Yang et al., 2020) with N-MORB defined by $La_N/Sm_N = 0.8$-1.5. The rhyolites are omitted from these and most trace element figures.

Figure 5. (a) LREE versus HREE ratios, normalized to the Primitive Mantle values of McDonough and Sun (1995). Ratios of 1.00 are chondritic. Most QVF lavas have LREE-depleted patterns with flat HREE, RA-N lavas are LREE-enriched with steeper HREE patterns. Others are intermediate. We attribute the steeper REE patterns in the north to more slab melt. The RA-S with La_N/Sm_N ~1.5 and Dy_N/Yb_N ratios ~1.00 actually have U-shaped HREE patterns; they are the high-Mg andesites. (b) Zr/Hf versus Sm/Hf ratios. Primitive Mantle ratios are shown for reference. Samples with Sm/Hf > 1.43 have negative Hf concentration anomalies. Note that most BAB and mBAB-N have higher Zr/Hf that overlap N- and E-MORB, and that many Havre Trough rocks, especially RA-N have medium to large negative Hf anomalies (Sm/Hf >1.7). (c) Ba/La versus Ce/Pb ratios: the slab component. The negative correlation reflects enrichment of Ba and Pb relative to LREE that increases from BAB to RA-S. Note that the relative Pb enrichment is greater in QVF than RA-S. Literature data sources as for Fig. 4. (d) REE patterns of a representative basalt (MgO>7%) of each type normalized to Primitive Mantle. By "S-shape" we mean the maxima at Nd and minima at Tm. The representative samples are: BAB, DR69-1; mBAB-N, DR113-1; mBAB-S, DR162-1A; RA-N, DR117-1; RA-S, DR162-19; QVF, DR170-2; CRH, DR7-1.

Figure 6. $^{143}Nd/^{144}Nd$ versus (a) Nb/Yb, (b) $^{87}Sr/^{86}Sr$, and (c) $^{176}Hf/^{177}Hf$. The three most enriched samples from the southernmost QVF volcanoes, Clark and Whakatane, are omitted. The red and blue circles and x's show mixing and melting models explained in the Fig. 4 caption. The offset of the alkali rhyolites (mBAB-NR) from the closest mBAB-N, that has Nb/Yb=1.5, reflects their extreme crystal fractionation. Literature data are from Barker et al. (2013), Gamble et al. (1996), Timm et al. (2014, 2016), Todd et al. (2011), and Woodhead et al. (2001). The MORB-EPR data in (c) are from Salters et al. (2011).

Figure 7. $^{206}Pb/^{204}Pb$ vs. $^{207}Pb/^{204}Pb$ (a), and $^{208}Pb/^{204}Pb$ (b). Data sources as in Figure 6 but only spiked literature data are plotted. The line is the Northern Hemisphere Reference Line. MORB data are from Niu et al. (1996, 1999) and Class and Lehnert (2012) for the EPR. Kermadec sediment data are from Gamble et al. (1996) and Todd et al. (2010), omitting samples with $^{206}Pb/^{204}Pb < 18.8$ that are diluted by arc-derived sediment. Torlesse sediment data are from Price et al. (2015).

Figure 8. Ce/Pb vs $^{206}Pb/^{204}Pb$ (a), and Nb/Yb (b). Binary mixing between sediment and the AMW forms a triangle from the bottom right to BAB and mBAB in (a). Only one of these samples has Ce/Pb as high as most MORB. Therefore, most are somewhat enriched in Pb relative to REE, presumably from a slab component. The near vertical trend for most samples indicates that both the mantle and slab components have similar $^{206}Pb/^{204}Pb$. The rough positive correlation in (b) indicates that the most common mantle in the Havre Trough is more Nb-rich than at the QVF. The correlation reflects increasing flux melting toward the origin. The alkali rhyolites (mBAB-NR) have twice the Nb/Yb ratio of the nearby mBAB basalt due to differentiation, but have not assimilated Pb from the crust because their Ce/Pb ratios have not decreased.

Figure 9. Bathymetric map of the newly documented caldera at 30°S in the middle of the Havre Trough. Contour intervals are 100 m. The dredge tracks end at the arrow tip. All samples are alkalic rhyolite.

Table 1. Chemical analyses and metadata for rock samples from the Havre Trough.

SO255	DR161-1	-32.82	179.67	RA-S	225	GL	ridge	2610	2164	EMP	LA-ICP-MS	53.07	1.06	16.28	8.82	0.12	6.22	10.88	3.26	0.18	0.10		98.26	5.26	36.8	276	71.8	33.3	36.5	99.1	80.8	15.4	3.21	146	22.6	61.1	0.538	0.160	80.7	2.38	7.22	1.27	6.96	2.38	0.924	3.24	0.555	3.80	0.823	2.43	0.354	2.38	0.348	1.71	0.040	1.10	0.210	0.064			0.703729	0.000006	0.512967	0.000005	6.57					18.7794	0.0010	15.5957	0.0009	38.5721	0.0022
SO255	DR161-4	-32.82	179.67	RA-S	225	WR	ridge	2610	2164	XRF	ICP-MS	51.12	0.85	18.16	9.12	0.19	5.71	11.66	2.46	0.59	0.15	1.33	99.25	5.35	33.6	278	13.4	36.0	25.1	50.1	72.0	15.0	11.1	249	20.5	53.1	0.698	0.288	136	5.79	12.9	2.00	10.1	2.97	1.05	3.45	0.558	3.50	0.719	1.97	0.294	1.93	0.295	1.41	0.043	0.571	0.237	0.703729			0.512987		9.43	0.283208		14.96	18.6913	0.0011	15.5807	0.0010	38.4459	0.0023
SO255	DR162-1A	-32.86	179.87	mBAB-S	205	WR	ridge	4002	3469	XRF	ICP-MS	51.23	0.65	17.04	6.55	0.12	8.87	13.17	2.07	0.24	0.06	0.86	99.26	3.98	37.8	207	407	36.4	148	58.1	46.9	12.6	3.49	118	17.0	46.1	0.452	0.107	23.9	1.43	4.85	0.734	4.74	1.68	0.666	2.25	0.411	2.80	0.598	1.69	0.256	1.69	0.263	1.18	0.042	0.58	0.082	0.058	0.702861	0.000005	0.513114	0.000005	8.01	0.283185		14.16	18.7907	0.0007	15.6085	0.0008	38.6078	0.0026
SO255	DR162-7	-32.86	179.87	mBAB-S	205	GL	ridge	4002	3469	EMP	LA-ICP-MS	52.69	0.81	16.67	7.03	0.15	7.35	12.38	2.75	0.11	0.07		97.09	4.74	36.0	219	127	31.4	56.7	89.2	65.3	14.0	1.66	112	19.0	54.2	0.534	0.117	32.0	1.60	5.49	0.97	5.54	1.89	0.740	2.64	0.460	3.16	0.693	2.09	0.296	2.03	0.298	1.53	0.039	0.766	0.092	0.030
SO255	DR162-19	-32.86	179.87	RA-S	205	GL	ridge	4002	3469	XRF	ICP-MS	51.60	0.87	16.66	8.19	0.15	8.09	11.44	2.47	0.40	0.10	0.88	99.45	4.75	37.0	268	306	38.8	141	68.6	61.5	14.6	6.88	170	19.7	56.9	0.990	0.253	90.8	3.47	9.18	1.44	7.51	2.33	0.860	2.85	0.499	3.29	0.696	1.95	0.293	1.93	0.297	1.44	0.052	1.53	0.509	0.147	0.703417	0.000006	0.513041	0.000005	8.01	0.283185		14.16	18.7907	0.0007	15.6085	0.0008	38.6078	0.0026
SO255	DR162-23	-32.86	179.87	mBAB-S	205	WR	ridge	4002	3469	XRF	ICP-MS	52.03	0.72	16.74	6.91	0.12	7.72	13.17	2.37	0.14	0.07		96.79	4.06	37.7	221	186	31.4	63.1	88.4	61.6	13.5	2.76	123	15.6	36.7	0.398	0.156	50.3	1.45	4.60	0.801	4.56	1.67	0.650	2.22	0.391	2.69	0.577	1.72	0.251	1.72	0.244	1.05	0.028	0.94	0.157	0.045
SO255	DR162-26	-32.86	179.87	mBAB-S	205	WR	ridge	4002	3469	XRF	ICP-MS	53.97	1.23	16.75	9.87	0.17	4.84	9.71	3.14	0.19	0.11	-0.04	99.18	7.43	35.4	354	5.36	33.6	10.1	58.4	72.2	16.8	2.33	170	26.7	77.0	0.901	0.113	88.4	3.11	9.54	1.58	8.61	2.90	1.11	3.75	0.683	4.46	0.944	2.66	0.401	2.61	0.404	1.96	0.069	0.85	0.352	0.124
SO255	DR164-1	-33.13	179.69	RA-S	210	GL	smt	1907	1561	EMP	LA-ICP-MS	52.69	0.97	15.23	9.77	0.19	6.51	11.25	2.97	0.30	0.11		94.03	5.04	42.3	304	39.3	36.0	29.3	137	87.5	14.8	6.12	182	20.4	63.2	0.937	0.314	127	3.75	9.95	1.50	7.52	2.30	0.881	2.96	0.510	3.47	0.751	2.22	0.332	2.26	0.331	1.61	0.077	2.27	0.509	0.135	0.703261	0.000005	0.513039	0.000006	7.98					18.7908	0.0014	15.6111	0.0012	38.6300	0.0030
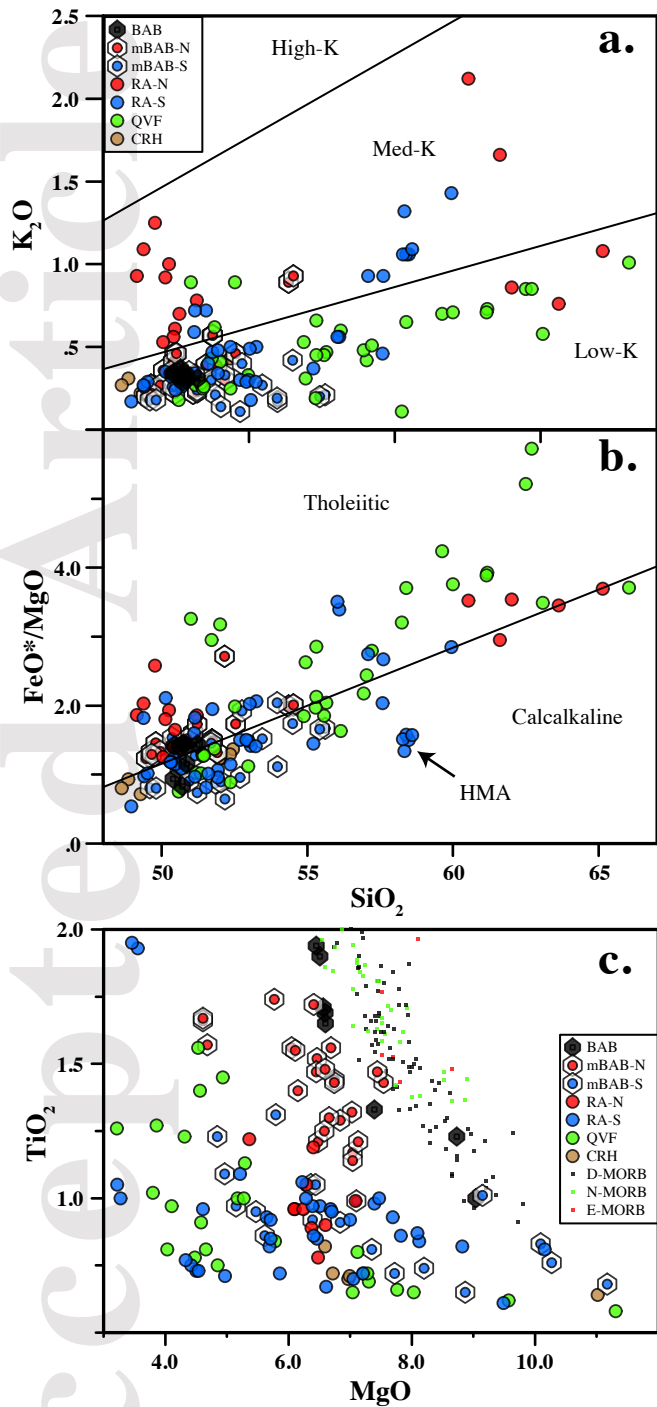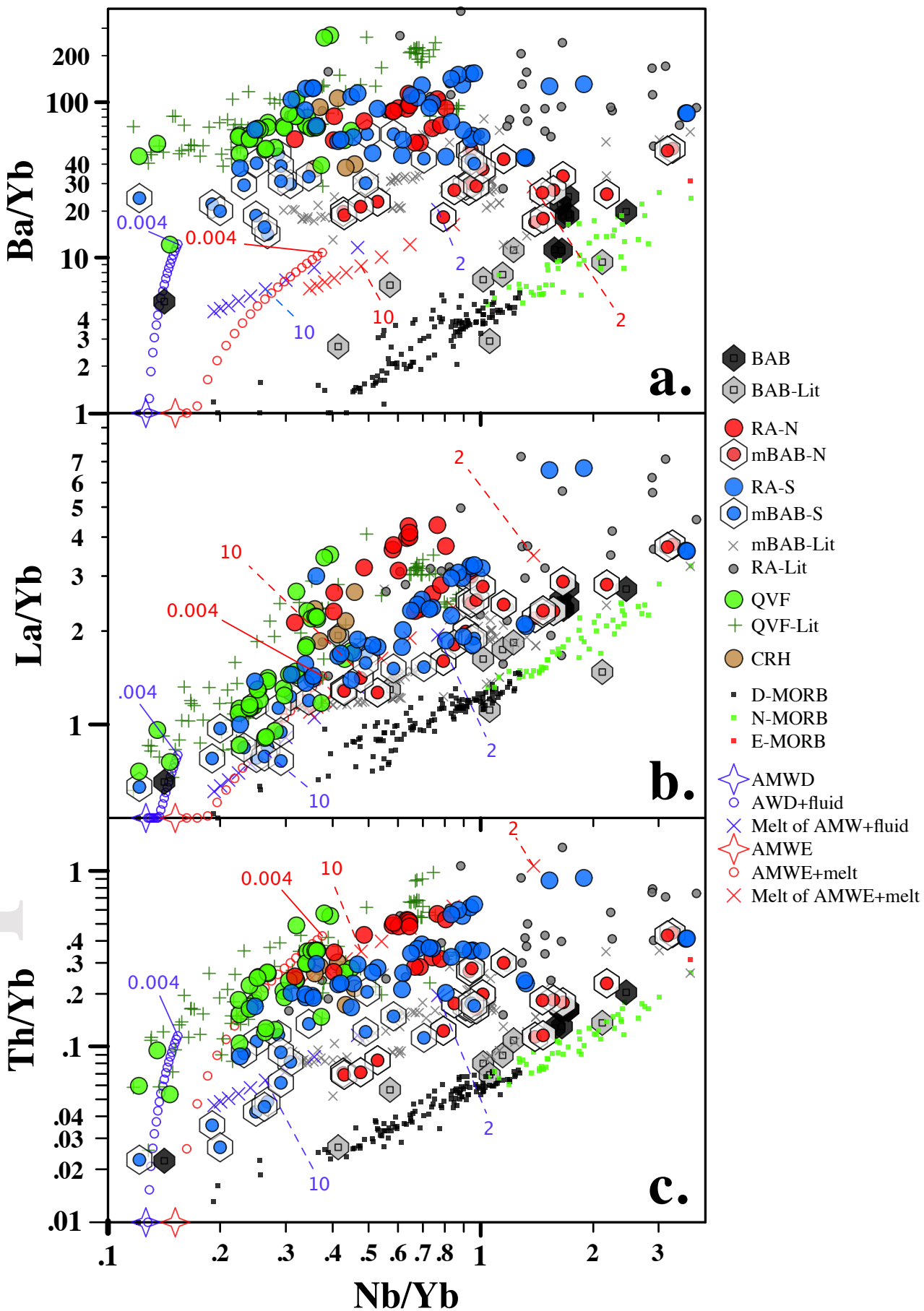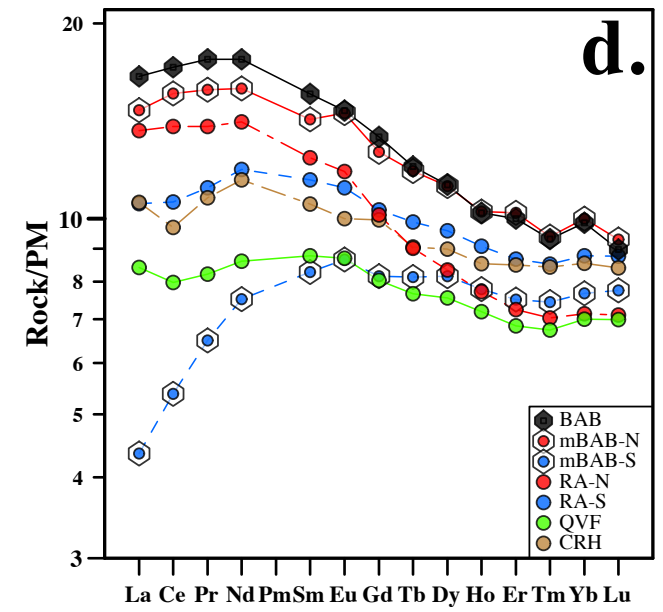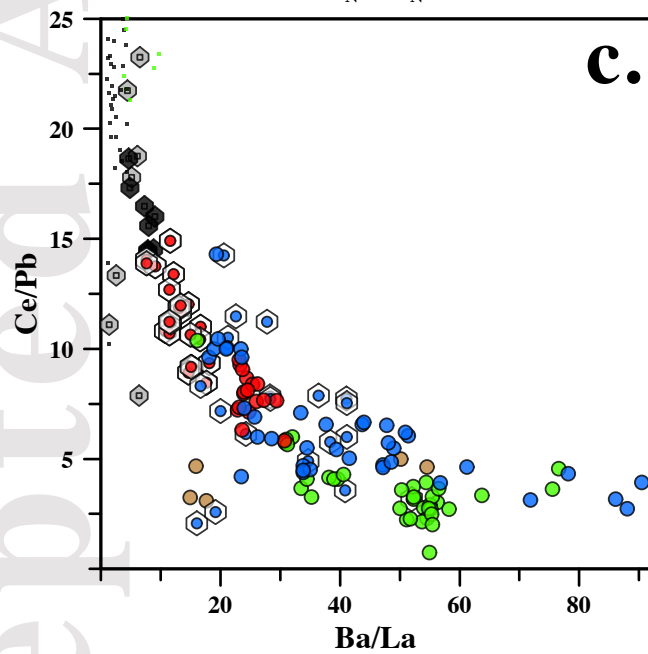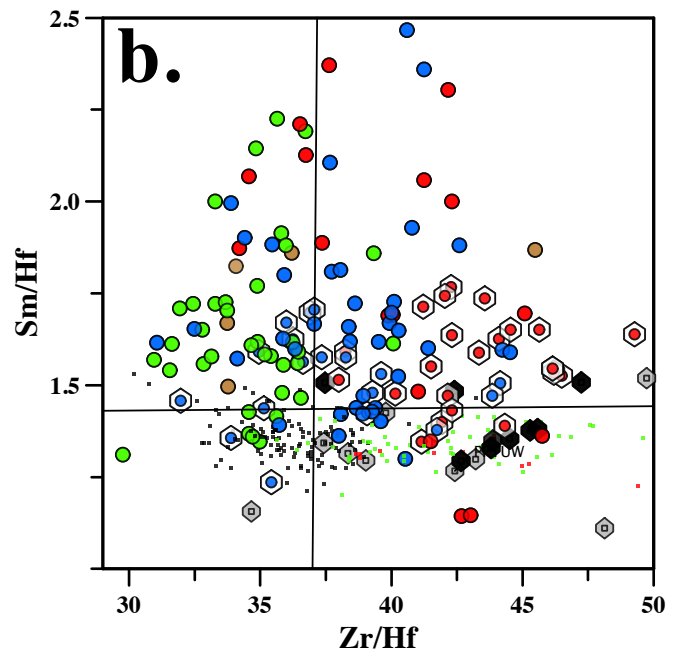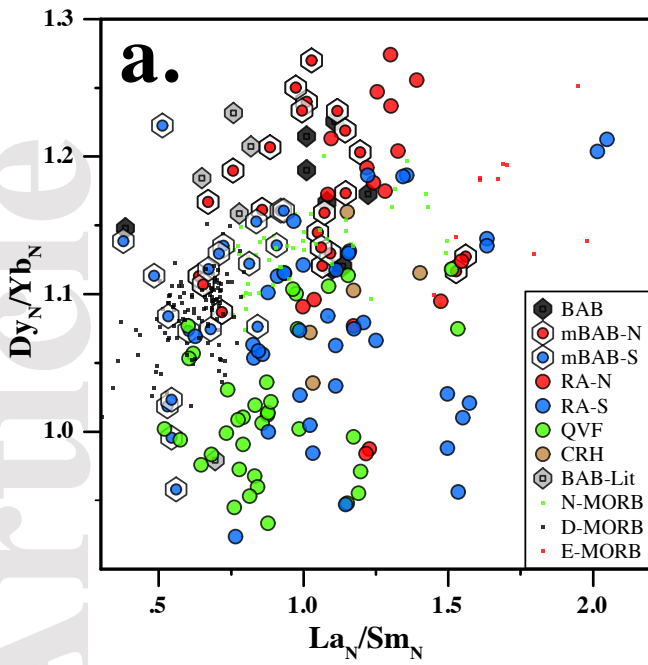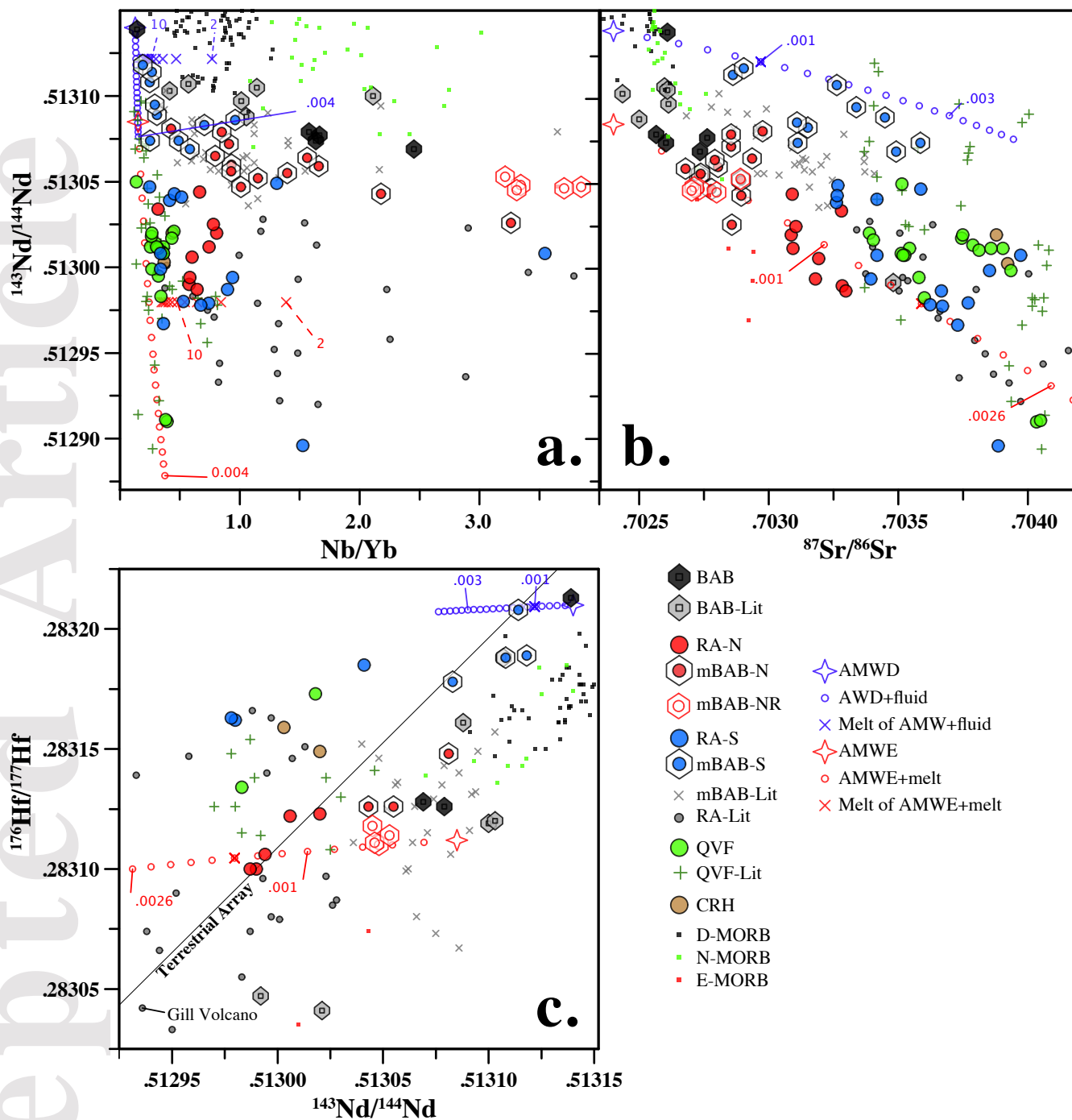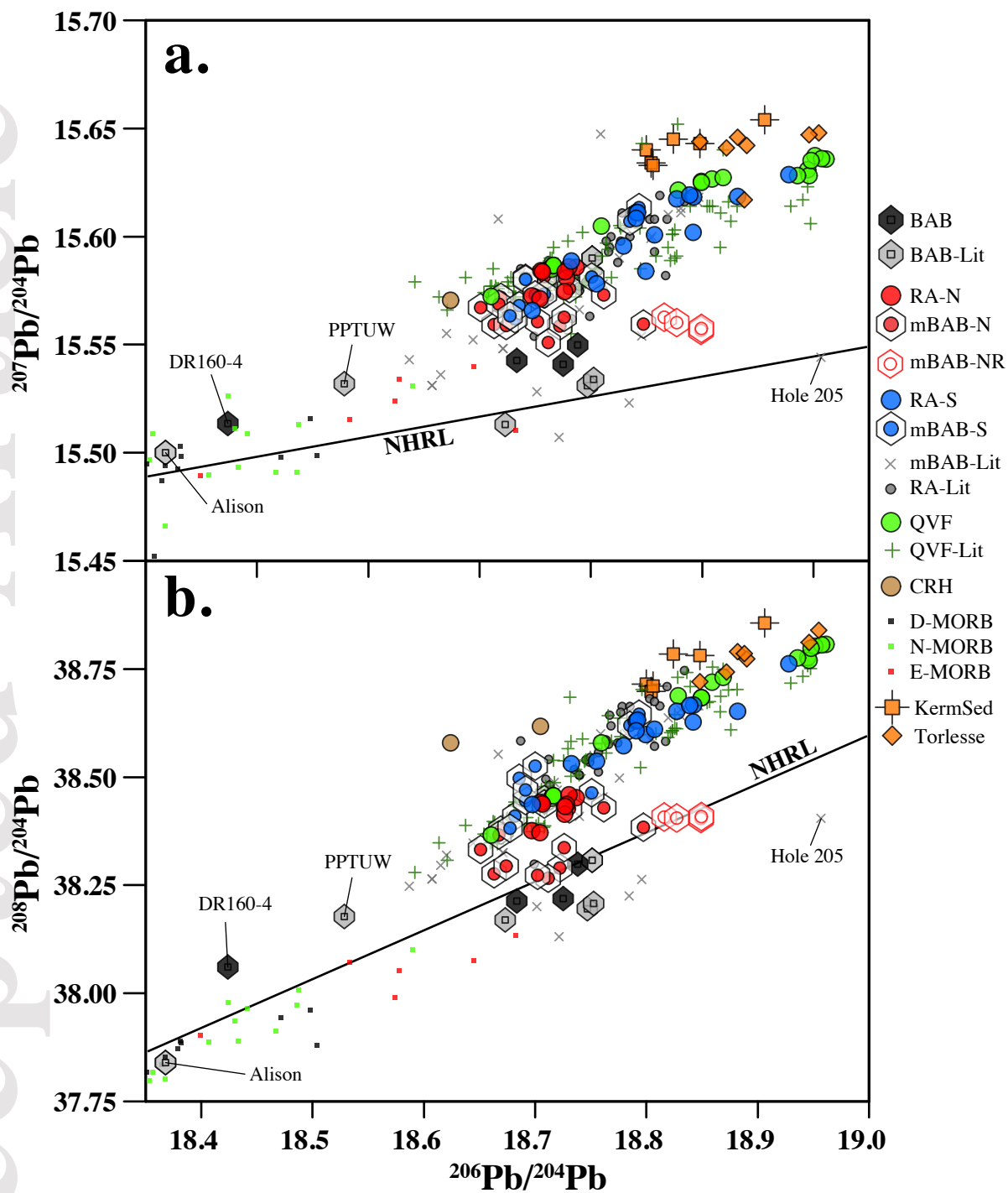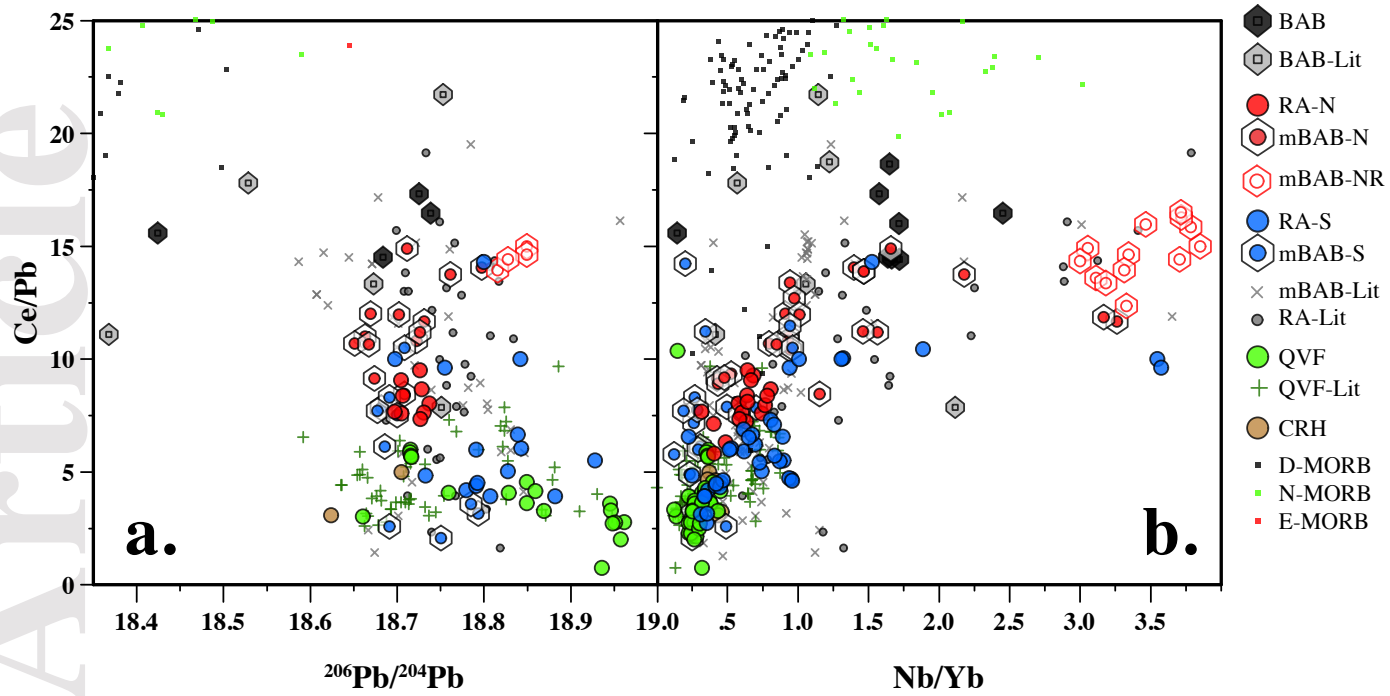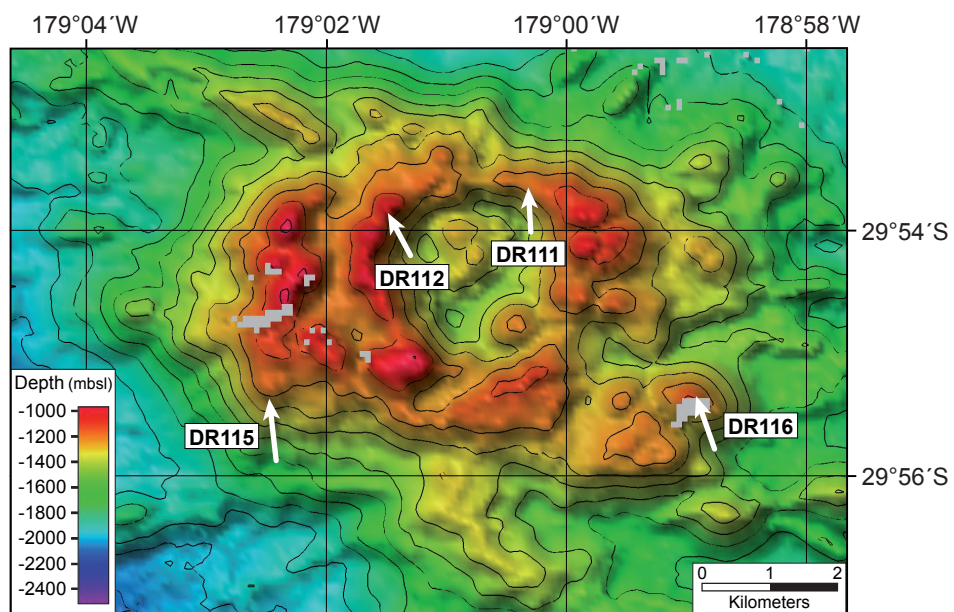SO255	DR164-5	-33.13	179.69	RA-S	210	GL	smt	1907	1561	XRF	ICP-MS	52.99	0.97	15.37	9.50	0.20	6.39	11.34	2.80	0.30	0.14		97.12	5.13	40.6	312	33.3	35.8	28.5	138	91.1	14.8	6.13	188	19.2	60.0	1.00	0.317	131	3.74	10.2	1.55	7.63	2.27	0.894	2.89	0.503	3.31	0.707	2.14	0.313	2.20	0.318	1.49	0.070	2.26	0.502	0.144	0.703264	0.000005	0.513043	0.000006	8.06					18.7922	0.0010	15.6111	0.0012	38.6323	0.0038
SO255	DR164-7A	-33.13	179.69	RA-S	210	GL	smt	1907	1561	EMP	LA-ICP-MS	53.23	0.95	15.14	9.44	0.18	6.70	11.30	2.66	0.20	0.12		99.13	5.03	42.9	301	45.7	36.0	34.4	137	83.2	14.4	5.97	179	20.1	61.9	0.917	0.316	125	3.69	9.73	1.51	7.63	2.34	0.876	3.07	0.523	3.42	0.741	2.23	0.322	2.18	0.327	1.59	0.067	2.17	0.499	0.142
SO255	DR165-1	-33.16	179.99	QVF	185	GL	smt	1407	1162	EMP	LA-ICP-MS	55.11	0.81	14.17	11.22	0.21	5.27	9.87	2.41	0.45	0.09		99.44	6.79	47.7	425	16.0	36.0	15.9	200	108	15.3	10.6	156	24.6	50.8	0.661	0.655	162	3.13	8.33	1.38	7.35	2.48	0.928	3.48	0.612	4.18	0.907	2.75	0.399	2.76	0.421	1.91	0.043	3.64	0.453	0.183
SO255	DR165-2	-33.16	179.99	QVF	185	WR	smt	1407	1162	XRF	ICP-MS	52.37	0.62	14.18	8.52	0.16	9.57	12.68	1.58	0.25	0.06	0.03	99.70	4.69	49.9	309	486	40.6	102	103	60.8	12.6	5.41	152	15.1	30.3	0.385	0.368	99	1.80	5.01	0.806	4.36	1.53	0.588	2.02	0.368	2.52	0.544	1.55	0.239	1.60	0.251	0.898	0.034	1.72	0.271	0.108
SO255	DR165-4	-33.16	179.99	QVF	185	GL	smt	1407	1162	EMP	LA-ICP-MS	55.65	1.00	14.56	10.54	0.18	5.17	10.04	2.28	0.47	0.10		98.53	6.26	44.8	415	11.7	32.9	14.2	186	125	15.9	9.87	166	22.2	46.6	0.642	0.582	153	2.99	8.22	1.30	7.13	2.41	0.895	3.35	0.526	3.88	0.826	2.32	0.382	2.61	0.389	1.40	0.041	3.67	0.463	0.164
SO255	DR165-6	-33.16	179.99	QVF	185	GL	smt	1407	1162	XRF	ICP-MS	56.93	0.81	16.67	8.76	0.18	4.03	9.10	2.92	0.48	0.11	0.44	99.45	8.59	33.5	267	34.8	28.0	20.7	107	73.3	16.1	9.71	188	25.6	61.2	0.789	0.712	188	3.48	9.54	1.50	7.92	2.62	0.939	3.38	0.612	4.16	0.899	2.58	0.398	2.67	0.419	1.68	0.059	3.44	0.555	0.208	0.703787	0.000004	0.513014	0.000005	7.48					18.9612	0.0007	15.6359	0.0007	38.8071	0.0021
SO255	DR165-9	-33.16	179.99	QVF	185	GL	smt	1407	1162	EMP	LA-ICP-MS	60.0	1.17	13.6	10.6	0.22	2.82	7.07	3.35	0.71	0.14		99.66	10.3	37.3	334	9.5	32.2	13.9	155	139	14.8	14.0	138	30.0	73.5	1.06	1.02	245	4.43	12.5	2.03	10.6	3.41	1.17	4.44	0.770	5.20	1.08	3.31	0.500	3.57	0.510	2.12	0.060	5.01	0.680	0.280
SO255	DR166-1	-33.13	-179.96	QVF	190	GL	smt	1736	1457	EMP	LA-ICP-MS	51.45	0.72	15.46	9.31	0.19	7.28	13.27	2.02	0.26	0.05		97.81	4.49	38.2	301	26.7	38.2	35.7	140	85.3	13.7	5.21	145	15.3	29.4	0.470	0.379	89.3	1.61	4.73	0.792	4.40	1.56	0.638	2.18	0.383	2.64	0.559	1.70	0.252	1.77	0.256	0.906	0.033	2.35	0.225	0.084	0.703749	0.000004	0.513020	0.000005	7.61	0.283173		13.71	18.9574	0.0007	15.6360	0.0007	38.8060	0.0022
SO255	DR166-2	-33.13	-179.96	QVF	190	WR	smt	1736	1457	XRF	ICP-MS	50.59	0.58	13.36	8.53	0.17	11.31	13.79	1.44	0.18	0.05	0.33	100.10	4.01	54.2	292	538	47.7	139	88.8	56.3	11.7	3.65	134	14.1	27.0	0.385	0.295	72.4	1.32	3.91	0.648	3.65	1.37	0.539	1.86	0.343	2.35	0.508	1.43	0.220	1.46	0.226	0.774	0.035	1.42	0.176	0.079	0.703744	0.000006	0.513018	0.000005	7.58	0.283173		13.71	18.9512	0.0011	15.6375	0.0009	38.8022	0.0024
SO255	DR166-4	-33.13	-179.96	QVF	190	GL	smt	1736	1457	EMP	LA-ICP-MS	51.4	0.72	15.5	9.39	0.18	7.22	13.1	1.98	0.26	0.05		99.85	4.81	48.3	286	232	37.9	35.7	130	85.4	13.9	5.00	147	16.0	31.0	0.410	0.36	85.1	1.56	4.62	0.78	4.53	1.58	0.610	2.18	0.440	2.94	0.600	1.96	0.270	1.82	0.280	0.980	0.030	2.01	0.190	0.080
SO255	DR166-10	-33.13	-179.96	QVF	185	GL	smt	1736	1457	EMP	LA-ICP-MS	51.41	0.69	15.49	9.29	0.18	7.30	13.34	2.01	0.25	0.05		97.79	4.30	36.8	281	35.3	35.7	34.6	130	75.9	13.5	5.00	147	14.6	28.5	0.468	0.356	85.4	1.59	4.48	0.781	4.28	1.46	0.611	2.14	0.363	2.51	0.545	1.57	0.237	1.67	0.243	0.846	0.031	2.09	0.208	0.080
SO255	DR167-5	-33.16	-179.96	QVF	185	WR	smt	793	555	XRF	ICP-MS	54.88	0.78	17.84	8.28	0.16	4.48	10.30	2.64	0.53	0.10	0.17	99.38	7.75	34.5	299	37.1	28.0	20.2	130	75.9	13.5	5.00	147	14.6	28.5	0.698	0.820	178	3.24	8.83	1.36	7.14	2.29	0.823	2.89	0.511	3.42	0.740	2.12	0.326	2.19	0.347	1.44	0.053	11.8	0.526	0.222	0.703811	0.000005	0.513011	0.000005	7.44					18.9359	0.0025	15.6281	0.0017	38.7757	0.0045
SO255	DR167-7	-33.16	-179.96	QVF	185	GL	smt	793	555	XRF	ICP-MS	56.15	0.81	17.30	7.60	0.15	4.66	10.08	2.52	0.60	0.11	0.51	99.03	6.19	36.6	312	33.4	27.0	18.8	137	105.8	15.0	15.1	197	23.5	55.8	0.733	0.879	202	3.47	9.51	1.47	7.88	2.40	0.871	3.17	0.565	3.80	0.819	2.33	0.361	2.40	0.380	1.54	0.055	3.49	0.567	0.429	0.703857	0.000005	0.513012	0.000004	7.44					18.9480	0.0015	15.6351	0.0005	38.7976	0.0014
SO255	DR167-9	-33.16	-179.96	QVF	190	WR	smt	793	555	XRF	ICP-MS	66.03	0.89	15.31	5.34	0.14	1.44	5.26	4.35	1.01	0.20	0.39	99.28	7.75	26.7	81	6.2	10.5	1.7	20.2	81.2	17.0	19.2	179	40.1	106	1.32	0.920	336	5.95	16.5	2.54	13.4	4.25	1.34	5.36	0.953	6.40	1.38	3.96	0.616	4.13	0.653	2.90	0.094	4.53	0.986	0.467
SO255	DR169-1A	-33.35	179.84	QVF	190	WR	Cole	2200	1791	EMP	LA-ICP-MS	55.58	1.13	14.46	9.81	0.19	5.29	10.08	2.86	0.45	0.15		98.14	6.00	42.3	361	53.3	28.1	14.2	114	99.2	15.8	8.96	177	23.7	64.6	1.17	0.428	155	4.40	11.4	1.75	8.89	2.80	1.05	3.63	0.615	4.15	0.859	2.57	0.372	2.71	0.384	1.80	0.077	3.48	0.715	0.236	0.703403	0.000005	0.513017	0.000004	7.56					18.8688	0.0005	15.6273	0.0009	38.7307	0.0030
SO255	DR169-2	-33.35	179.84	QVF	190	GL	Cole	2200	1791	EMP	LA-ICP-MS	52.97	0.80	16.66	7.96	0.16	7.12	11.62	2.29	0.33	0.09	0.28	99.47	5.28	40.9	300	244	33.3	73.5	72.7	64.3	15.0	6.27	203	19.1	52.9	0.867	0.325	127	3.33	8.76	1.32	6.78	2.13	0.804	2.67	0.471	3.17	0.676	1.92	0.292	1.93	0.300	1.32	0.065	2.11	0.537	0.191	0.703388	0.000005	0.513021	0.000004	7.63					18.8591	0.0005	15.6298	0.0006	38.7194	0.0018
SO255	DR169-12A	-33.35	179.84	QVF	185	GL	Cole	2200	1791	EMP	LA-ICP-MS	57.04	1.23	14.46	10.52	0.20	4.31	8.80	2.90	0.42	0.13		98.49	6.35	43.8	414	7.2	31.4	11.6	120	118	16.5	8.27	146	27.4	68.1	1.13	0.454	119	3.55	10.1	1.62	8.55	2.81	1.04	3.98	0.695	4.68	1.00	2.93	0.438	3.05	0.462	1.90	0.074	2.76	0.448	0.157
SO255	DR170-2	-33.41	179.87	QVF	185	GL	Cole	1480	1094	EMP	LA-ICP-MS	51.17	0.65	15.96	8.27	0.15	8.03	13.74	1.68	0.27	0.08	0.32	99.13	4.82	48.0	295	200	39.4	66.3	80.4	57.3	14.2	4.47	187	15.4	33.3	0.525	0.276	108	2.77	6.90	1.06	5.42	1.78	0.669	2.22	0.387	2.59	0.552	1.54	0.232	1.54	0.237	0.930	0.043	1.69	0.456	0.172	0.703600	0.000005	0.512983	0.000005	6.89	0.283134		12.35	18.8284	0.0013	15.6215	0.0010	38.6881	0.0029
SO255	DR170-4	-33.41	179.87	QVF	195	WR	Cole	1480	1094	XRF	ICP-MS	51.35	0.66	16.07	7.89	0.15	7.76	14.02	1.74	0.28	0.07	0.91	99.52	5.04	49.3	285	221	37.0	61.1	84.6	51.2	13.4	5.86	177	14.9	33.1	0.509	0.270	108	2.66	6.65	1.03	5.33	1.73	0.666	2.15	0.383	2.53	0.541	1.52	0.229	1.50	0.234	0.920	0.042	1.55	0.445	0.143
SO255	DR174-1	-33.84	179.56	mBAB-S	195	GL	basin	3630	3322	EMP	LA-ICP-MS	53.46	1.31	15.99	8.79	0.19	5.79	10.29	3.79	0.27	0.14		98.31	6.04	36.7	289	133	28.1	32.7	85.6	86.0	16.2	4.34	195	24.7	89.3	1.82	0.162	112	3.96	11.6	1.87	9.53	2.95	1.11	3.83	0.642	4.20	0.904	2.65	0.377	2.59	0.383	2.14	0.122	1.48	0.290	0.102	0.703151	0.000004	0.513063	0.000005	8.83	0.283178		13.89	18.6817	0.0023	15.5620	0.0017	38.4097	0.0042
SO255	DR174-1	-33.84	179.56	mBAB-S	170	WR	basin	3630	3322	XRF	XRF	51.87	1.15	17.33	8.54	0.15	6.48	10.73	3.22	0.36	0.15	1.00	99.23
TAN0206	DR02A-14-4	-30.21	-178.45	QVF	162	GL	Macauley	335	n.a.	EMP	LA-ICP-MS	73.09	0.90	11.49	5.15	0.15	0.48	2.51	4.17	1.86	0.19		99.57	10.9	19.0	24.0	6.30	0.200	15.7	103	15.5	25.9	193	46.2	149	1.88	0.960	362	11.3	29.7	4.44	22.2	6.15	1.70	7.07	1.16	7.49	1.57	4.86	0.740	5.17	0.760	4.31	0.120	4.95	1.82	0.73	0.703543	0.000004	0.513012	0.000005	7.46					18.7155	0.0008	15.5856	0.0008	38.4556	0.0018
TAN0206	DR02A-18-1a	-30.21	-178.45	QVF	162	GL	Macauley	650	n.a.	EMP	LA-ICP-MS	71.85	0.87	12.41	4.98	0.18	0.51	3.03	4.26	1.70	0.19		99.51	11.8	19.0	20.0	0.550	5.30	0.200	15.6	106	15.8	28.5	199	52.7	170	2.00	1.08	387	12.5	31.1	4.71	23.8	6.54	1.81	7.79	1.30	8.46	1.78	5.48	0.840	5.70	0.880	4.86	0.120	5.29	2.00	0.76	0.703511	0.000005	0.513009	0.000004	7.40					18.7147	0.0008	15.5848	0.0007	38.4515	0.0023
TAN0206	DR02A-19-16	-30.21	-178.45	QVF	162	GL	Macauley	630	n.a.	EMP	LA-ICP-MS	72.59	0.90	12.00	4.99	0.14	0.40	2.71	4.27	1.83	0.16		99.52	11.6	19.0	20.0	0.530	5.41	0.260	17.9	108	15.4	26.0	193	50.6	158	1.89	1.09	361	11.7	29.8	4.50	22.9	6.25	1.77	7.47	1.25	8.01	1.69	5.27	0.800	5.26	0.840	4.57	0.120	5.30	1.88	0.75	0.703525	0.000003	0.513008	0.000004	7.37					18.7159	0.0003	15.5864	0.0008	38.4568	0.0023
TAN0206	DR02A-20-1	-30.21	-178.45	QVF	162	GL	Macauley	640	n.a.	EMP	LA-ICP-MS	72.49	0.95	11.59	5.51	0.18	0.46	2.53	4.19	1.87	0.22		99.48	11.7	17.9	20.0	0.530	5.41	0.260	17.9	183	10.0	30.0	452	22.6	6.27	1.66	7.19	1.18	7.84	1.45	5.12	0.770	5.37	0.800	4.61	0.130	5.30	1.88	0.76	0.703518	0.000005	0.513008	0.000004	7.38					18.7164	0.0005	15.5866	0.0005	38.4572	0.0016

Technical abbreviations: WR = whole rock, GL = glass, mbsl = meters below sea level, wt% = g/100g, ppm = μg/g, LOI = loss on ignition, SUM = original total of XRF analysis with Fe as Fe₂O₃, n.a. = not analyzed

Technical notes: All major elements shown on a volatile free basis. Measured Fe₂O₃ converted to FeO prior to volatile free normalization

Method abbreviations: XRF = X-Ray Fluorescence, EMP = Electron Microprobe, ICP-MS = Solution Inductively Coupled Mass Spectrometry, LA-ICP-MS = Laser Ablation ICP-MS

Isotope analysis methods: All Sr-Nd-Pb isotope ratios by thermal ionization mass spectrometry (TIMS), all Hf isotope ratios by multi-collector ICP-MS. Sample data reported relative to NBS987 87Sr/86Sr = 0.710250 ± 8 (2SD,
N=101), La Jolla 143Nd/144Nd = 0.511850 ± 6 (2SD, N=95), NBS981 206Pb/204Pb = 16.9408 ± 18, 207Pb/204Pb = 15.4975 ± 18, 208Pb/204Pb = 48 (2SD, N=173), SPEX 179Hf/177Hf = 0.282170 ± 6 (2SD, N=110).

*εNd and εHf use CHUR values of Bouvier, A., Vervoort, J. D., and Patchett, P. J., 2008, The Lu-Hf and Sm-Nd isotopic composition of CHUR: Constraints from unequilibrated chondrites and implications for the bulk composition of terrestrial planets: Earth and Planetary Science Letters, v. 273, no. 1, p. 48-57.